PHYSICAL REVIEW D **85,** 024007 (2012)

Viscous damping of r-modes: Small amplitude instability

Mark G. Alford, Simin Mahmoodifar, and Kai Schwenzer
Department of Physics, Washington University,
St. Louis, Missouri 63130, USA
(Received 25 March 2011; revised manuscript received 30 November 2011; published 6 January 2012)

We study the viscous damping of r-modes of compact stars and analyze in detail the regions where small amplitude modes are unstable to the emission of gravitational radiation. We present general expressions for the viscous damping times for arbitrary forms of interacting dense matter and derive general semi-analytic results for the boundary of the instability region. These results show that many aspects, such as the physically important minima of the instability boundary, are surprisingly insensitive to detailed microscopic properties of the considered form of matter. Our general expressions are applied to the cases of hadronic stars, strange stars, and hybrid stars, and we focus on equations of state that are compatible with the recent measurement of a heavy compact star. We find that hybrid stars with a sufficiently small core can ''masquerade'' as neutron stars and feature an instability region that is indistinguishable from that of a neutron star, whereas neutron stars with a core density high enough to allow direct Urca reactions feature a notch on the right side of the instability region.

DOI: 10.1103/PhysRevD.85.024007 PACS numbers: 04.30.Db

I. INTRODUCTION

Pulsars rotate with periodicities whose stability exceeds that of any terrestrial clock. Pulsar frequencies and their time derivatives are thereby by far the most accurately measured properties of compact stars, whereas all other information about them is subject to much greater uncertainties. Correspondingly it is extremely tempting to exploit this information in order to learn about their internal structure and, in particular, whether they consist of novel phases of dense matter that might contain deconfined quarks [1]. This requires the development of unique signatures that connect particular microscopic properties to the macroscopic data.

Pulsar frequencies can change over time both by accretion of matter that transfers angular momentum from a companion star and by the emission of gravitational radiation due to oscillations of the star. A particularly interesting class of oscillation modes are r-modes [2–4] which are counter-rotating modes of a rotating star and are in the absence of viscous damping unstable at all rotation frequencies [5]. This instability transforms rotational into gravitational wave energy and leads to an exponential rise of the r-mode amplitude. When viscous damping is taken into account the star is stable at low frequencies but there remains an instability region at high frequencies [6,7]. If this instability is stopped at a large amplitude, r-modes are a strong and continuous source of gravitational waves and could provide an extremely efficient mechanism for the spin-down of a young compact star [8,9]. Observational data for spin frequencies of pulsars, that spin down and allow the determination of an approximate age associated to their spin-down rate,[1] is shown in Fig. 1. Whereas observed old pulsars in binary systems can spin nearly as fast as the maximum Kepler frequency, above which the binding force cannot counteract the centrifugal pseudoforce anymore, and can feature rotation periods in the millisecond range, younger stars are far below this limit. This is surprising since in their creation during a supernova a significant fraction of the angular momentum of the initial star should be taken over by the much smaller compact core which therefore should dramatically spin up. This naive assumption is backed up by explicit analyses where millisecond rotation frequencies at birth are indeed possible [10]. If r-modes spin down compact stars on time scales shorter than the age of the youngest observed pulsar, the lower boundary of the instability window should give an upper limit for the maximum rotation frequency of young compact stars.[2]

R-modes are also relevant for the case of older stars in binaries that are spun up by accretion since they generally limit the maximum possible rotation frequency of a star to

[1]The spin-down age is determined by the assumption that magnetic dipole breaking, which features a qualitatively similar behavior as gravitational wave emission, dominates the spin-down. It can thereby only give a rough order of magnitude estimate for the age. Age estimates are, in particular, not available for stars that currently spin up and which are correspondingly not included in the plot. However, for the youngest stars there are independent age determinations from the observation of the corresponding supernova remnant that qualitatively agree with these estimates.

[2]Note that the final frequency of the spin-down evolution can lie below the minimum of the instability boundary since the damping of the r-mode can take some time to complete, even after it enters the stable regime.

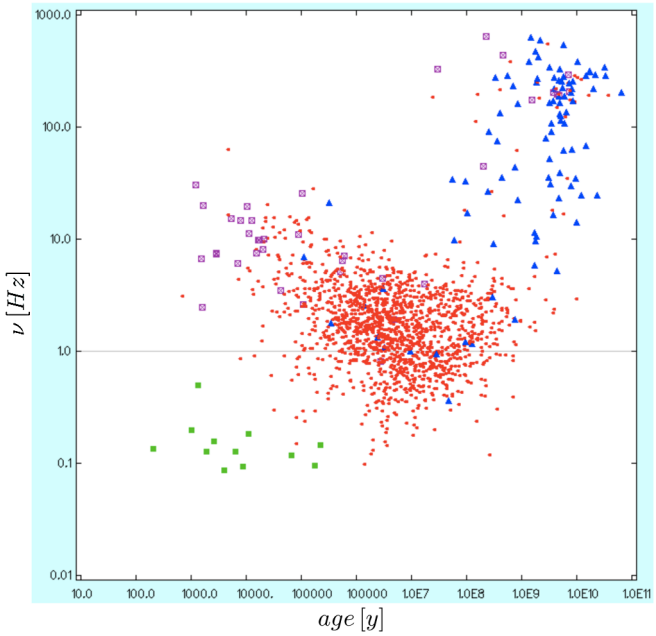

FIG. 1 (color online). Rotation frequencies of observed pulsars versus their approximate spin-down age from the ATNF pulsar catalogue [49].

values substantially below the Kepler frequency. A challenging finding is that, in contrast to purely hadronic stars, more exotic possibilities like self-bound strange stars [11], hybrid stars [7] or stars where hyperons are present in the core [12] can feature so-called ''stability windows'' where over a range of intermediate temperatures the r-mode instability is absent up to rather high frequencies. The observation of stars rotating at such frequencies could therefore provide evidence for exotic phases in their interior. In this context the masses and radii of stars provide further important information. The recent precise measurement of a heavy compact star with $M \approx 2M_\odot$ [13,14] puts constraints on the presence of exotic phases since such phases lead to a softening of the equation of state which in general leads to a smaller maximum mass that is achievable for such an equation of state. In combination with pulsar data this should lead to more restrictive bounds on the possible presence of certain forms of matter in compact stars.

A major problem for the extraction of information on the composition of compact stars from observational data is the huge theoretical uncertainty in the equation of state of dense matter and its transport properties. This holds both for the hadronic side, where nuclear data is only available at low densities and large proton fractions, and also for hypothetical phases of quark matter, since QCD as the fundamental theory of strong interactions cannot be solved so far in this nonperturbative regime. Another big uncertainty factor is the crust of the neutron star since although its microscopic physics is in general more constrained by experimental data than the high density phases in the core, its structural complexity limits so far a complete description. Simplified estimates suggest that the crust could have a strong impact on the damping of r-mode oscillations via surface rubbing at the crust-core interface [15]. However, as in all present analyses, r-modes are considered as solutions to the hydrodynamics equations of an ideal fluid. When certain regions feature viscosities that are enhanced by orders of magnitude, like at the crust-core interface, the r-mode profile should strongly change in these regions and the reduced amplitude there would result in a considerably weaker damping. Therefore, we neglect crust effects in our present analysis, but a more complete understanding of these effects in the future is desirable. Unfortunately due to all this, even if two phases feature significant qualitative differences these are often overshadowed by the huge quantitative uncertainties in the detailed microscopic properties of either of them. However, it was previously observed that certain features, like the important case of the minimum of the instability region can be surprisingly insensitive to quantitative details of the considered models [6]. If such statements can be substantiated this could allow us to devise robust signatures of the qualitative features that can be stringently tested with present and forthcoming astrophysical data.

To this end, we study in this paper the instability regions of small amplitude r-modes in detail. In contrast to previous treatments that studied particular star models numerically, we derive general analytic results that are valid for stars consisting of various forms of matter and compare these to numeric evaluations for realistic equations of state. We find that although the form of the instability region can be qualitatively distinct for the different forms of matter, many aspects of the instability regions are extremely insensitive to the detailed unknown microscopic input, like the transport coefficients of a given phase. Moreover, we reveal the parametric dependence on the underlying microscopic parameters where such dependences are significant. We study explicitly the cases of neutron stars, strange stars as well as hybrid stars and in view of the recent discovery of a $2M_\odot$ compact star, we generally apply only equations of state that can accommodate such a heavy star. We find that the instability regions of the hybrid stars are almost indistinguishable from those of neutron stars if the size of the quark matter core is smaller than roughly half of the star's radius. Further, we also study the case of an ultraheavy neutron star where direct Urca reactions are allowed in the core and find that it features a notch at the right hand side of the instability region. Finally, in addition to the dominant $m = 2$ r-mode we also consider higher multipoles and note that they could easily be excited and become important for the evolution of the star.

In a companion paper [16] we show that due to the strong increase of the bulk viscosity with amplitude [17–20] the r-mode instability is only present at sufficiently small amplitudes and the exponential r-mode growth is

eventually saturated at finite amplitudes so that r-modes could indeed provide a viable mechanism for both the spin-down of young stars and the frequency limit of old, accreting stars.

II. STAR MODELS AND R-MODES

A. Static star models

The analysis of compact star oscillations and their damping requires as a first step the stable equilibrium configuration of the star. In this section we will discuss the considered star models that are used later on. The equilibrium star configuration is determined by the gravitational equations for a fluid sphere. We employ here the general relativistic Tolman-Oppenheimer-Volkov (TOV) equations [21]. The latter require the equation of state of neutral and β-equilibrated dense matter. The recent measurement of a neutron star with the large mass $1.97 \pm 0.04 M_\odot$ [13,14] puts bounds on the equation of state of dense matter. We generally study equations of state that can accommodate such a heavy star. We consider three qualitatively different classes and study in each case both a star model with a standard value of $1.4 M_\odot$ and one with a large mass $2 M_\odot$:

(1) Neutron stars (NS) are obtained for an equation of state that is hadronic at all relevant densities. Whereas the above maximum mass does not pose problems for neutron stars obtained from most hadronic equations of state, it seem nearly impossible to obtain such heavy stars which contain a significant amount of hyperonic matter [14]. Therefore we do not study this possibility here and consider only stars consisting of neutrons, protons and electrons as well as muons at sufficiently high density. We also neglect the possible presence of hadronic pairing which in general significantly reduces the bulk viscosity [22,23]. Such pairing is only realized in certain shells within the star and as long as they are not large this might not qualitatively change the results obtained here. However, the intricate dynamics of a two-component fluid can change this simplistic picture [24]. For our numerical results we employ the equilibrated equation of state by Akmal, Pandharipande and Ravenhall (APR) [25] which relies on a potential model that reproduces scattering data in vacuum supplemented by a model for three-body interactions in order to reproduce the saturation properties at nuclear densities. As a low density extension of the APR data we use [26,27]. Furthermore, we study in this class also a neutron star with an ultrahigh mass $2.21 M_\odot$ close to the mass limit for the APR equation of state, since in this case direct Urca interactions are possible in the interior of the star leading to a significantly enhanced weak rate, cf. e.g. [17].

(2) Hybrid stars (HS) with an outer hadronic part and a core of quark matter are obtained from an equation of state where at some density the effective degrees of freedom change from hadrons to quarks. In general the equation of state of interacting quark matter is unknown and there are only hints from the perturbative regime [28–30] or model studies. We use the simple quartic parameterization for the equation of state of ungapped 3-flavor quark matter [17,31] in terms of the individual quark chemical potentials μ_d, μ_u and μ_s and the electron chemical potential μ_e

$$p_{\rm par} = \frac{1-c}{4\pi^2}(\mu_d^4+\mu_u^4+\mu_s^4) - \frac{3m_s^2\mu_s^2}{4\pi^2} + \frac{3m_s^4}{32\pi^2}\left(3+4\log\left(\frac{2\mu_s}{m_s}\right)\right) - \mathcal{B} + \frac{\mu_e^4}{12\pi^2}, \quad (1)$$

where c, m_s and B are effective model parameters that incorporate some effects of the strong interactions between the quarks. From this equation of state we find the β equilibrated and charge neutral ground state which depends on a single quark number chemical potential μ_q. We use the general form since the computation of transport properties below requires susceptibilities around the equilibrium state. Within the parameterization Eq. (1) the recent measurement of a heavy star strongly restricts the equation of state so that only equations of state that are strongly interacting ($c > 0.3$) are compatible [14,31]. These are equations of state where the transition to quark matter is at rather low values of the baryon number $\lesssim 1.5 n_0$, where n_0 is nuclear matter density, and we choose here one where it occurs at $1.5 n_0$. Since the APR equation of state happens to be very similar to the above form Eq. (1) so that even multiple transitions are possible [31], we do not expect the transition density to be a robust result that is independent of the considered equations of state. Therefore we study here in addition also two $1.4 M_\odot$ hybrid star models obtained with quark equations of state that cannot accommodate a heavy star when combined with the APR equation of state. Ona has a small quark core, obtained for a transition density of $3.25 n_0$, and the other a medium-sized quark core, obtained for a transition density of $3 n_0$. There are many possible phases of quark matter that feature various color superconducting pairing patterns. Here we do not explicitly study star models with pairing, but note that the parameterization Eq. (1) can also describe superconducting matter. For our hybrid star models we make the assumption of local charge neutrality, excluding the possibility of a mixed phase and thereby circumventing the description of the wealth of possible geometric structures of such a mixture.

(3) Strange stars (SS) that are self-bound could exist according to the strange matter hypothesis [32] that the true ground state of strongly interacting matter is 3-flavor quark matter. For strange stars we use the same equation of state Eq. (1), but use parameter sets that realize the strange matter hypothesis. In contrast to the case of hybrid stars large mass strange stars are possible even for $c = 0$ and due to our ignorance of the precise form of the interacting equation of state we choose this value to keep our model as simple as possible. For a strange quark mass of $m_s = 150$ MeV stable strange stars exist in this case for bag constants $B_{\rm lim} < (158\ {\rm MeV})^4$, whereas heavy strange stars exist for this mass value only for bag constants $B \lesssim (140\ {\rm MeV})^4$. Lower effective quark mass values or changes in the quartic term ($c \neq 0$) relax these bounds.

We note already at this point that although the detailed parameters we chose here for our star models are rather arbitrary, we will give general analytic expressions below that will reveal the dependence of our main results on the various model parameters. The characteristic parameters of the considered star models are given in Table I. As is a well known property, the radii of the different models vary only moderately with the mass for masses of 1 to $2M_\odot$. The density profiles are shown in Fig. 2. The core densities of these star models range from below $3n_0$ to more than $7n_0$. In contrast to neutron and hybrid stars that vary in density by 14 orders of magnitude, strange stars feature a roughly constant density profile.

TABLE I. Results of the considered models of neutron stars (NS), strange stars (SS) and hybrid stars (HS). Shown are the mass of the star M, the mass of the core $M_{\rm core}$, the radius R, the baryon density at the center of the star n_c given in units of nuclear saturation density n_0, the average density $\langle n\rangle$ and the Kepler frequency Ω_K. The neutron stars were obtained by solving the relativistic TOV equations for catalyzed neutron matter using the APR equation of state [25] with low density extension [26,27] and the strange stars with a quark gas bag model with $c = 0$, $m_s = 150$ MeV and a bag parameter $B = (138\ {\rm MeV})^4$. Large mass hybrid stars are only found when strong interaction corrections are considered, cf. [31], and we find a $2M_\odot$ star for $c = 0.4$, $m_s = 140$ MeV, $B = (137\ {\rm MeV})^4$. The additional two $1.4M_\odot$ hybrid models with smaller cores, marked with an asterisk, result from equations of state that do not allow large mass models. They correspond to $c = 0$, $m_s = 150$ MeV, $B = (164.5\ {\rm MeV})^4$ and $(171.5\ {\rm MeV})^4$ which are chosen to obtain transition densities of $3n_0$ and $3.25n_0$, respectively.

	$M[M_\odot]$	$M_{\rm core}[M_\odot]$	R[km]	$n_c[n_0]$	$\langle n\rangle[n_0]$	Ω_K[kHz]
NS	1.4	(1.39)	11.5	3.43	1.58	6.02
	2.0	(1.99)	11.0	4.91	2.46	7.68
	2.21	0.85	10.0	7.17	3.37	9.31
SS	1.4	-	11.3	2.62	1.91	6.17
	2.0	-	11.6	4.95	2.43	7.09
HS	1.4(S)	0.38*	10.8	5.89	1.85	6.61
	1.4(M)	0.66*	10.3	6.66	2.09	7.06
	1.4(L)	1.06	12.7	2.32	1.17	5.16
	2.0	1.81	12.2	4.89	1.84	6.62

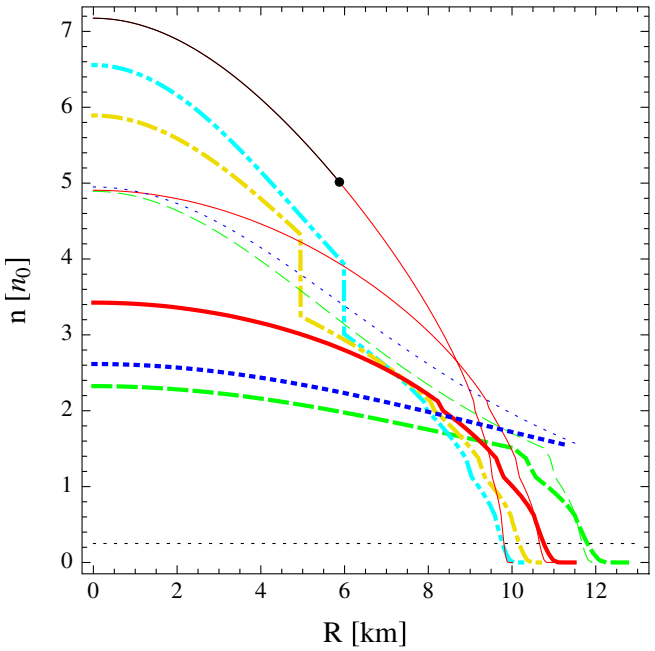

FIG. 2 (color online). The density profiles of the star models considered in this work. The solid lines represent neutron star models with an APR equation of state, the dotted lines represent strange stars with a bag model equation of state and the dashed, dot-dot-dashed and dot-dashed lines represent hybrid star models with large, medium and small quark matter cores, respectively. Thick lines represent $1.4M_\odot$ stars and thin lines represent massive $2M_\odot$ stars. In contrast to strange stars that are basically homogeneous, stars that contain hadronic matter have a very strong density dependence that extends over 14 orders of magnitude reflected by the near zero segments in this plot. The very thin solid curve presents the maximum neutron star model for the APR equation of state $\sim 2.2M_\odot$ where hadronic direct Urca processes are allowed to the left of the dot. The dotted horizontal line denotes the density $n = n_0/4$ chosen as the beginning of the crust whose contribution is not taken into account in the damping time integrals below.

B. R-mode profile

The analysis of oscillation modes of compact stars requires the solution of the corresponding hydrodynamics equations [4]. Whereas the solution of the general relativistic equations for static star models is straightforward, the corresponding dynamic equations are more involved and explicit analytic expressions for the r-mode oscillation are only available in nonrelativistic approximation. Yet numerical analyses of the general relativistic equations show that except for very compact stars the relativistic corrections are moderate [33–35]. In the nonrelativistic case the current state of the art is the comprehensive

analysis [3]. It might therefore seem more consistent to employ Newtonian equations for the static star models as well, but we prefer to perform the necessary approximation for the oscillation at least around the correct equilibrium configuration. In particular since we study heavy quark and hybrid stars where the different approximations could differ. In particular in the large amplitude regime, a consistent general relativistic analysis would clearly be desirable. Furthermore, so far these analyses assume that the oscillation modes are solutions of an ideal fluid. For these modes the damping is then computed in a second step.

R-modes are normal oscillations of rotating stars and correspondingly they require as a first step the solution of a uniformly rotating stellar model. Since neutron stars are cold, dense systems we assume a barotropic fluid where the pressure p is only a function of the energy density ρ. The hydrodynamic Euler equation for this spherical system, determining the enthalpy h and the equation for the gravitational potential Φ of the star, have to be solved with appropriate boundary conditions [3]. To simplify the demanding analysis a slow rotation expansion is performed and, since the density fluctuation of the r-mode vanishes to leading order in the expansion, the computation of bulk viscosity damping times requires an expansion of h, Φ and of the energy density ρ to next-to-leading order

$$X(r,\cos\theta) = X_0(r) + X_2(r,\cos\theta)\left(\frac{\Omega^2}{\pi G\bar{\rho}_0}\right) + \cdots,$$

where X stands for either of the three quantities, Ω is the angular velocity of the rotation and $\bar{\rho}_0$ the average energy density of the corresponding nonrotating star. The main effect of the rotational corrections is a flattening of the star due to centrifugal forces.

The next step is the search for eigenmodes of the rotating star in a linear low amplitude approximation, e.g. for the conserved baryon number $\Delta n \ll \bar{n}$. They can completely be described by the change in the gravitational potential $\delta\Phi$ and the hydrodynamical perturbation

$$\delta U = \frac{\delta p}{\rho} - \delta\Phi.$$

These are likewise expanded to next-to-leading order in Ω in the form

$$\delta X(r,\cos\theta) = R^2\Omega^2\left(\delta X_0(r) + \delta X_2(r,\cos\theta)\frac{\Omega^2}{\pi G\bar{\rho}_0} + \cdots\right),$$

where δX stands again either for $\delta\Phi$ or δU and R is the radius of the static star. The potentials obey complicated differential equations with corresponding boundary conditions given in [3]. The boundary conditions require that the oscillation frequencies ω_r in the rotating and ω_i in the inertial frame are connected to the rotation frequency Ω via

$$\omega_r \equiv \omega = \kappa(\Omega)\Omega, \qquad \omega_i = m\Omega - \omega_r, \tag{2}$$

where the parameter κ can likewise be expanded in Ω

$$\kappa = \kappa_0 + \kappa_2\frac{\Omega^2}{\pi G\bar{\rho}_0} + \cdots$$

We study classical r-modes which are a one parameter class of eigenmode solutions, $l = m$, that are to leading order determined by $\kappa_0 = 2/(m+1)$ and given by

$$\delta U_0(\vec{r}) = \sqrt{\frac{m}{\pi(m+1)^3(2m+1)!}}\alpha\left(\frac{r}{R}\right)^{m+1} P^m_{m+1}(\cos\theta)e^{im\varphi}$$

in terms of associated Legendre polynomials P^m_{m+1} and with the definition of the dimensionless amplitude α introduced in [6]. For the lowest r-mode that couples to gravitational waves with $m = 2$ the oscillation frequency in the inertial frame is given by $\omega_i = -4/3\Omega$, corresponding to a counter-rotating flow. The leading order gravitational potential obeys a differential equation that is given in appendix A where its analytic solution is given in the special case that the star is of uniform density. In general it requires a numeric solution and then completely determines the r-mode to this order.

At next-to-leading order there are two qualitatively different effects: First the connection between oscillation and rotation frequency as described by the parameter κ becomes nonlinear via a nonvanishing value of κ_2 that has to be obtained numerically from a corresponding differential equation [3]. In Fig. 3 the solution is shown for the star models discussed here. Whereas the corrections are small for quark stars, at large frequency they can become sizable for hadronic and hybrid stars. The second effect is the change of the potentials arising as solutions of rather

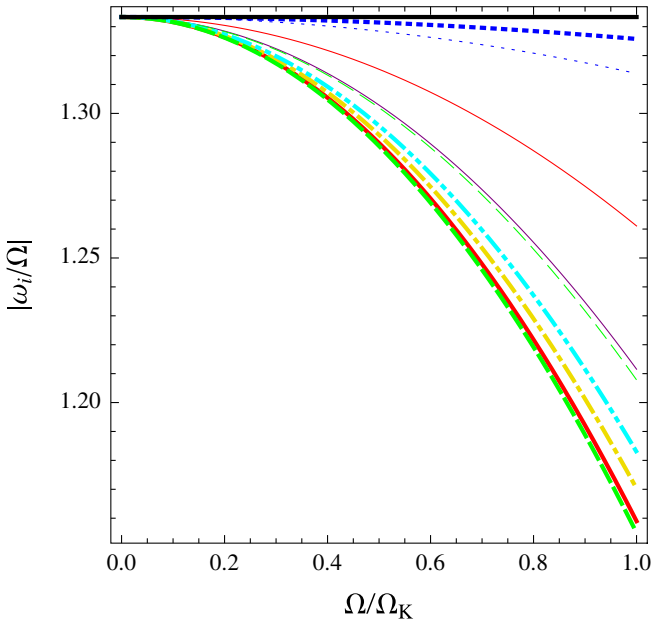

FIG. 3 (color online). Connection of the oscillation frequency ω_i of the r-mode in the inertial frame to the rotation frequency of the considered star models to next-to-leading order in the Ω-expansion. The horizontal line shows the leading order result and the conventions for the other curves are the same as in Fig. 2.

involved partial differential equations. At next-to-leading order they feature nontrivial radial and angular dependences that are not described by simple power laws or spherical harmonics anymore.

We are interested in the amplification of these modes due to gravitational waves and their viscous damping which are described by the energy dissipation

$$\frac{dE}{dt} = -\omega(\omega - m\Omega)^{2m+1}|\delta J_{mm}|^2 - \int d^3x(2\eta\delta\sigma^{ab}\delta\sigma_{ab} + \zeta\delta\sigma\delta\sigma^*), \quad (3)$$

where η and ζ are the shear and bulk viscosity, respectively. The fluctuations δJ_{mm} and $\delta\sigma_{ab}$ couple to gravitational waves and shear viscosity, respectively. The fluctuation $\delta\sigma \equiv \vec{\nabla}\cdot\delta\vec{v}$ of an r-mode oscillation which is subject to dissipation via bulk viscosity reads

$$\delta\sigma = -i\frac{2AR^2\Omega^3}{m+1}(\delta U_0 + \delta\Phi_0 + \cdots) + O(\Omega^5), \quad (4)$$

where A denotes the inverse speed of sound

$$A \equiv \frac{\partial\rho}{\partial p}\bigg|_0 \quad (5)$$

evaluated at equilibrium and the dots represent several further terms of next-to-leading order in Ω given in [3]. The terms in the parenthesis depend on the expansion coefficients of the potentials and on the connection parameter κ, but are by virtue of the expansion independent of frequency. The fluctuation $\delta\sigma$ is finally connected to the fluctuations of energy $\Delta\rho$ and baryon number density Δn via their continuity equations

$$|\delta\sigma| = |\vec{\nabla}\cdot\delta\vec{v}| = \kappa\Omega\left|\frac{\Delta\rho}{\bar{\rho}}\right| = \kappa\Omega\left|\frac{\Delta n}{\bar{n}}\right|.$$

Following [7], in our numerical analysis we will consider the change of κ at second order, but because of the involved numerics [3], we will not take into account all explicit second order terms in Eq. (4). A standard approximation [6] is to replace the Lagrangian density fluctuation by the Eulerian one which corresponds to neglecting the terms denoted by the parenthesis in Eq. (4). E.g. the density fluctuation for a $m = 2$ r-mode reads then to leading order

$$\left|\frac{\Delta\rho}{\bar{\rho}}\right| \approx \left|\frac{\delta\rho}{\bar{\rho}}\right| = \sqrt{\frac{8}{189}}\alpha AR^2\Omega^2\left(\left(\frac{r}{R}\right)^3 + \delta\Phi_0(r)\right)Y_3^2(\theta,\phi) \quad (6)$$

in terms of the spherical harmonics Y_3^2. However, we will give general semi-analytic expressions below that *are* valid to full next-to-leading order. These show that the influence of the neglected terms on important aspects of the instability regions is rather mild.

III. VISCOSITIES OF DENSE MATTER

A. General expressions

The bulk viscosity describes the local dissipation of energy in a fluid element which arises from the global oscillation mode of the star within a compression and rarefaction cycle. The integration over the whole star yields then the corresponding energy dissipation of the mode as will be discussed in the next section. Recently the bulk viscosity of large amplitude oscillations [18] has been studied in detail [17]. There it was shown that large amplitude oscillations are in general considerably more strongly damped and this mechanism can thereby saturate unstable r-modes at finite amplitudes as will be discuss in a companion article. In this article, however, we restrict ourselves to the subthermal regime $\mu_\Delta \ll T$ which determines whether small amplitude r-modes are initially unstable.

The bulk viscosity is maximal when the external oscillation frequency matches the time scale of the microscopic interactions that establish equilibrium. The relevant interactions in the case of star oscillations are slow weak processes. The parametric form of the beta-equilibration rate is given by

$$\Gamma^{(\leftrightarrow)} = -\tilde{\Gamma}T^\delta\mu_\Delta\left(1 + \sum_{j=1}^{N}\chi_j\left(\frac{\mu_\Delta^2}{T^2}\right)^j\right), \quad (7)$$

where $\mu_\Delta \equiv \sum_i\mu_i - \sum_f\mu_f$ is the quantity that is driven out of equilibrium due to the oscillations and its re-equilibration leads to the bulk viscosity. In the subthermal regime, $\mu_\Delta \ll T$, the nonlinear terms in the rate of the equilibration processes can be neglected, leading to the general analytic result for the subthermal bulk viscosity [17]

$$\zeta^< = \frac{C^2\tilde{\Gamma}T^\delta}{\omega^2 + (B\tilde{\Gamma}T^\delta)^2} = \zeta^<_{\max}\frac{f}{1+f^2} \quad (8)$$

in terms of the reduced weak rate $\tilde{\Gamma}$ and the strong susceptibilities B and C

$$C \equiv \bar{n}\frac{\partial\mu_\Delta}{\partial n}\bigg|_x, \qquad B \equiv \frac{1}{\bar{n}}\frac{\partial\mu_\Delta}{\partial x}\bigg|_n \quad (9)$$

as well as the oscillation frequency ω (in the rotating frame) and temperature T. It has a characteristic resonant form and as long as the combination of susceptibilities C^2/B does not vary too quickly with temperature, the subthermal viscosity has a maximum

$$\zeta^<_{\max} = \frac{C^2}{2\omega B} \quad \text{at} \quad T_{\max} = \left(\frac{\omega}{\tilde{\Gamma}B}\right)^{1/\delta} \quad (10)$$

and simple asymptotic limits

$$\zeta^< = \zeta^<_{\max}\cdot\begin{cases} f & (f \ll 1) \\ \frac{1}{f} & (f \gg 1) \end{cases},$$

where $f \equiv B\tilde{\Gamma}T^\delta/\omega$ can be identified as the feedback term in the differential equation that determines the damped oscillation [17].

TABLE II. *Upper panel:* Parameters of the general parameterization of the weak rate Eq. (7) for different processes of particular forms of matter which determine the damping due to bulk viscosity. The coefficients χ_i parameterize the nonlinear dependence on the chemical potential fluctuation μ_Δ arising in the suprathermal regime of the viscosity which is relevant for large amplitude r-modes studied in [16] but which are not relevant in this work. *Lower panel:* Parameters arising in the parameterization Eq. (11) of the shear viscosity for different strong and electromagnetic interaction processes. The leptonic and quark scattering arises from a non-Fermi liquid enhancement due to unscreened magnetic interactions.

Weak process	$\tilde{\Gamma}[\mathrm{MeV}^{(3-\delta)}]$	δ	χ_1	χ_2	χ_3
Quark nonleptonic	$6.59\times10^{-12}(\frac{\mu_q}{300\ \mathrm{MeV}})^5$	2	$\frac{1}{4\pi^2}$	0	0
Hadronic direct Urca	$5.24\times10^{-15}(\frac{xn}{n_0})^{1/3}$	4	$\frac{10}{17\pi^2}$	$\frac{1}{17\pi^4}$	0
Hadronic modified Urca	$4.68\times10^{-19}(\frac{xn}{n_0})^{1/3}$	6	$\frac{189}{367\pi^2}$	$\frac{21}{367\pi^4}$	$\frac{3}{1835\pi^6}$

Strong/EM process	$\tilde{\eta}[\mathrm{MeV}^{(3+\sigma)}]$	σ
Quark scattering	$1.98\times10^{9}\alpha_s^{-(5/3)}(\frac{\mu_q}{300\ \mathrm{MeV}})^{14/3}$	$\frac{5}{3}$
Leptonic scattering	$1.40\times10^{12}(\frac{xn}{n_0})^{14/9}$	$\frac{5}{3}$
nn-scattering	$5.46\times10^{9}(\frac{\rho}{m_N n_0})^{9/4}$	2

The shear viscosity arises from strong or electromagnetic interactions. In contrast to the bulk viscosity, the shear viscosity of dense matter is independent of the frequency of an external oscillation and approximately depends on temperature via a simple power law. Shear viscosity becomes large at low temperatures and therefore it is the dominant process for damping of the r-modes of cooler stars. Thereby, to leading order it can be parameterized as

$$\eta = \tilde{\eta} T^{-\sigma} \tag{11}$$

by simply factoring out the temperature dependence with exponent σ. In general several processes can contribute so that the full shear viscosity can approximately be written as a sum of such power laws for the individual processes.

B. Viscosities for the considered forms of matter

In the following we discuss the viscosities for the phases of dense matter present in the considered classes of compact stars. We note however, that the general results given here likewise apply to more complicated forms of matter like hyperonic and/or superfluid nuclear matter as well as various forms of superconducting quark matter.

1. Bulk viscosity

The general expression for the bulk viscosity Eq. (8) depends on the weak rates. In the case of hadronic matter in the absence of hyperons the weak equilibration occurs via the Urca channel

$$n \to p + e^- + \bar{\nu}_e, \qquad p + e^- \to n + \nu_e.$$

There are two qualitatively different cases depending on whether the direct process [36,37] is possible or only the modified version [37–39] where by-stander nucleons are necessary to satisfy energy momentum conservation. The latter represents a particular strong interaction vertex correction to the above process. However, from the point of view of the weak interaction these different processes belong to the same channel. Further, there is in principle also a corresponding process with muon instead of electrons. Since the phase space and thereby the rate of this process is strongly suppressed compared to the electron version at moderate densities we do not consider it here.

In strange quark matter the dominant channel for beta equilibration is the nonleptonic flavor changing process

$$s + u \leftrightarrow d + u,$$

whereas the corresponding quark Urca processes are parametrically suppressed in $T/\mu \ll 1$. The weak parameters $\tilde{\Gamma}$, δ and χ in the parameterization of the weak rate Eq. (7) are given on the uuper panel of Table II.

Further, the inverse speed of sound A, Eq. (5), as well as the strong susceptibilities B and C, Eq. (9), that parameterize the deviation from chemical equilibrium are required. In order to make it easy to apply our general results to different forms of interacting hadronic matter, we implement the APR equation of state using the simple parameterization employed in [40] to approximate the dependence of the energy per particle on the proton fraction x by a quadratic form

$$E(n, x) = E_s(n) + S(n)(1 - 2x)^2,$$

where E_s and S are the corresponding energy for symmetric matter and the symmetry energy for which we employ simple quadratic fits to the APR data. For comparison we also consider the susceptibilities in the approximation of a hadron gas which had been used in previous analyses of the

TABLE III. Strong interaction parameters, defined in Eqs. (5) and (9), describing the response of the particular form of matter. In the case of interacting hadronic matter a quadratic ansatz in the proton fraction x parameterized by the symmetry energy S is employed. The expressions for a hadron and quark gas are given to leading order in n/m_N^3 respectively next-to-leading order in m_s/μ.

	A	B	C
Hadronic matter	$m_N(\frac{\partial p}{\partial n})^{-1}$	$\frac{8S}{n}+\frac{\pi^2}{(4(1-2x)S)^2}$	$4(1-2x)(n\frac{\partial S}{\partial n}-\frac{S}{3})$
Hadronic gas	$\frac{3m_N^2}{(3\pi^2 n)^{2/3}}$	$\frac{4m_N^2}{3(3\pi^2)^{1/3}n^{4/3}}$	$\frac{(3\pi^2 n)^{2/3}}{6m}$
Quark matter (gas: $c=0$)	$3+\frac{m_s^2}{(1-c)\mu_q^2}$	$\frac{2\pi^2}{3(1-c)\mu_q^2}(1+\frac{m_s^2}{12(1-c)\mu_q^2})$	$-\frac{m_s^2}{3(1-c)\mu_q}$

bulk viscosity [7,36,39]. Likewise we compute these quantities for the generic, phenomenological form of the equation of state of interacting quark matter Eq. (1). The resulting strong interaction parameters describing the response of the different models are given in Table III.

2. Shear viscosity

In previous r-mode analyses the shear viscosity in hadronic matter has been approximated by the contribution from strong hadron-hadron-scattering using the fit in [41] to the standard low density ($\lesssim n_0$) data given in [42]

$$\eta_n = 347\rho^{9/4}T^{-2}\,\frac{\mathrm{g}}{\mathrm{cms}}, \tag{12}$$

where T is in units of Kelvin and ρ is given in $\mathrm{g/cm^3}$. Extrapolating this fit to high densities relevant for neutron stars overestimates the viscosity. The new evaluation in [43] shows instead that due to a non-Fermi liquid enhancement arising from the exchange of Landau-damped transverse photons, the main contribution to the shear viscosity of hadronic matter, at temperatures relevant to the spin-down evolution of the compact stars, comes from electron scattering and is given by

$$\eta_e = 4.26\times 10^{-26}(xn)^{14/9}T^{-(5/3)}\,\frac{\mathrm{g}}{\mathrm{cms}}, \tag{13}$$

where T is in Kelvin and the baryon number density n is in units of $\mathrm{cm^{-3}}$. In the calculation of η_e we have only considered electron-electron and electron-proton scattering and neglected the small effect of the muons to the shear viscosity. For densities larger than nuclear matter saturation density this electron contribution dominates over the hadronic one down to temperatures below 10^7 K. This region contains the part of the instability region that is relevant for the spin-down evolution of stars. Therefore in our main analysis we will completely neglect the hadronic component of the shear viscosity. However, we will compare with the previous form of the shear viscosity Eq. (12) in order to discuss the effect of our improved analysis on the instability region.[3]

[3]The left-most part of the instability region below $\sim 10^7$ K only features an instability at very large frequencies. This part would only be relevant for old stars that are spun up by accretion, yet frequencies very close to the Kepler frequency are not reached via this mechanism anyway, cf. Fig. 1, due to turbulent effects.

In the case of ungapped quark matter, the shear viscosity is dominated by quark-quark scattering, and in the limit of $T \ll q_D$, where q_D is the Debye wave number, it is given by [44]

$$\eta_q = \frac{1}{40\pi a}\left(\frac{2N_q}{\pi}\right)^{1/3}\alpha_s^{-(5/3)}\mu_q^{14/3}T^{-(5/3)}, \tag{14}$$

where $\alpha_s = \frac{g^2}{4\pi}$ is the QCD coupling constant, $a \simeq 1.81$, $N_q = 3$ and μ_q and T are in units of MeV. The temperature dependence arises again from a non-Fermi liquid enhancement of the quark interaction. These expressions yield the parameters in the parameterization of the shear viscosity Eq. (11) as given on the lower panel of Table II.

IV. R-MODE TIME SCALES

A. General expressions

The amplitude of the r-mode oscillations evolves with time dependence $e^{i\omega t - t/\tau}$, where ω is the real part of the frequency of the r-mode and $1/\tau$ is the imaginary part of the frequency. The latter describes both the exponential rise of the r-mode driven by the Friedman-Schutz mechanism [45] and its decay due to viscous damping. We can decompose $1/\tau$ as

$$\frac{1}{\tau(\Omega,T)} = \frac{1}{\tau_G(\Omega)} + \frac{1}{\tau_B(\Omega,T)} + \frac{1}{\tau_S(T)},$$

where τ_G, τ_B and τ_S are gravitational radiation, bulk viscosity and shear viscosity time scales, respectively. The lowest of these individual time scales determines if the r-mode is unstable or damped. The damping time for the individual mechanisms is in general given by

$$\frac{1}{\tau_i} \equiv -\frac{1}{2E}\left(\frac{dE}{dt}\right)_i \tag{15}$$

and requires both the total energy of the r-mode

$$E = \frac{1}{2}\alpha^2 R^4\Omega^2\int_0^R \rho(r)\left(\frac{r}{R}\right)^{2m+2}dr \tag{16}$$

and the dissipated energy which is given by the corresponding part of Eq. (3) [3]. For instance the dissipated energy Eq. (3) due to the bulk viscosity reads

$$\left(\frac{dE}{dt}\right)_\zeta = -\kappa^2\Omega^2\int d^3x\left|\frac{\Delta\rho}{\rho}\right|^2\zeta\left(\left|\frac{\Delta\rho}{\rho}\right|^2\right),$$

where the dependence of the bulk viscosity on the conserved number density fluctuation amplitude has been expressed in terms of the conserved energy density. If the star consists of several shells consisting of different forms of matter with different viscosity, as is the case for hybrid stars, neutron stars with a high density core where direct Urca reactions are allowed, etc., the integral consists of partial integrals over the individual shells s and the inverse viscous damping times can be written as

$$\frac{1}{\tau_i} = \sum_s \frac{1}{\tau_i^{(s)}}.$$

Therefore, the contribution of the different shells enters additively. We will in the following expressions suppress the explicit label (s) but implicitly assume that the damping times consist of several contributions when different layers are present. With these expressions the individual r-mode time scales can be obtained. The time scale of the r-mode growth due to gravitational wave emission is given by [6]

$$\frac{1}{\tau_G} = -\frac{32\pi(m-1)^{2m}}{((2m+1)!!)^2}\left(\frac{m+2}{m+1}\right)^{2m+2}\tilde{J}_m GMR^{2m}\Omega^{2m+2} \tag{17}$$

with the radial integral constant

$$\tilde{J}_m \equiv \frac{1}{MR^{2m}}\int_0^R \rho(r) r^{2m+2} dr. \tag{18}$$

1. Shear viscosity damping time

The damping time of an r-mode with angular quantum number m due to shear viscosity is given by

$$\frac{1}{\tau_S} = \frac{(m-1)(2m+1)}{\tilde{J}_m MR^{2m}}\int_0^R \eta r^{2m} dr.$$

Using the parameterization Eq. (11) this can be written as

$$\frac{1}{\tau_S} = \frac{(m-1)(2m+1)\tilde{S}_m \Lambda_{\rm QCD}^{3+\sigma} R}{\tilde{J}_m M T^{\sigma}} \tag{19}$$

in terms of the dimensionless constant

$$\tilde{S}_m \equiv \frac{1}{R^{2m+1}\Lambda_{\rm QCD}^{3+\sigma}}\int_{R_i}^{R_o} \tilde{\eta} r^{2m} dr, \tag{20}$$

where R_i and R_o are the inner and outer radius of the corresponding shell, if there are several ones. This constant contains the complete dependence on the particular microscopic processes. To make this quantity dimensionless the generic scale $\Lambda_{\rm QCD}$ has been introduced that is chosen as $\Lambda_{\rm QCD} = 1$ GeV for the numeric values. For the fundamental $m = 2$ r-mode the parameter $\tilde{S}$ is given for the different star models considered here in Table IV.

2. Bulk viscosity damping time

The bulk viscosity damping time is given by

$$\frac{1}{\tau_B} = \frac{\kappa^2}{\alpha^2 \tilde{J}_m MR^2}\int d^3x \left|\frac{\Delta n}{\bar{n}}\right|^2 \zeta\left(\left|\frac{\Delta n}{\bar{n}}\right|^2\right), \tag{21}$$

TABLE IV. Radial integral parameters and characteristic points of the instability region of a $m = 2$ r-mode for the star models considered in this work. The constant $\tilde{J}$, $\tilde{S}$, $\tilde{V}$ and $\tilde{W}$ are given by Eqs. (18), (20), (27), and (28) using the generic normalization scales $\Lambda_{\rm QCD} = 1$ GeV and $\Lambda_{\rm EW} = 100$ GeV. The temperatures and frequencies are obtained with the analytic expressions for the minima Eqs. (B2), (B3), (B8), and (B9) and for the maxima Eqs. (B5) and (B6). The expressions for a generic strange star (or quark core) in terms of the parameters of the quark model equation of state Eq. (1), using the constants $\hat{\Gamma}$ and $\hat{\eta}$ defined in Eq. (32) are given as well.

Star model	Shell	$\tilde{J}$	$\tilde{S}$	$\tilde{V}$	$\tilde{W}$	$T_{\rm min}[K]$	$\Omega_{\rm min}[Hz]$	$T_{\rm max}[K]$	$\Omega_{\rm max}[Hz]$
NS $1.4M_\odot$	Core	1.81×10^{-2}	7.68×10^{-5}	1.31×10^{-3}	1.61×10^{-6}	3.49×10^{9}	371	…	…
NS $1.4M_\odot$ gas			4.32×10^{-6}	1.28×10^{-4}	1.76×10^{-7}	3.70×10^{9}	226	…	…
NS $2.0M_\odot$		2.05×10^{-2}	2.25×10^{-4}	1.16×10^{-3}	1.72×10^{-6}	4.19×10^{9}	368	…	…
NS $2.21M_\odot$	d.U. core	2.02×10^{-2}	5.05×10^{-4}	1.16×10^{-8}	7.11×10^{-7}	2.03×10^{9}	493	…	…
	m.U. core			9.34×10^{-4}	1.55×10^{-6}				
SS Eq. (1)	All	$\frac{3}{28\pi}$	$\frac{\hat{\eta}\mu_q^{14/3}}{5\Lambda_{\rm QCD}^{14/3}\alpha_s^{5/3}}$	$\frac{\Lambda_{\rm EW}^4\hat{\Gamma}m_s^4\mu_q^3}{9\Lambda_{\rm QCD}^7(1-c)^2}$	$\frac{m_s^4}{4\pi^4\Lambda_{\rm EW}^4\Lambda_{\rm QCD}\hat{\Gamma}\mu_q^3}$	Equation (34)	Equation (33)	Equation (36)	Equation (35)
SS $1.4M_\odot$		3.08×10^{-2}	3.49×10^{-6}	3.53×10^{-10}	0.191	7.86×10^{6}	1020	1.01×10^{9}	8340
SS $2.0M_\odot$		2.65×10^{-2}	4.45×10^{-6}	3.38×10^{-10}	0.157	8.58×10^{6}	955	8.07×10^{8}	6600
HS $1.4M_\odot$ L	Quark core	1.93×10^{-2}	2.19×10^{-6}	1.38×10^{-10}	1.03×10^{-2}	9.87×10^{6}	1170	5.83×10^{8}	7270[a]
	Hadr. core		6.72×10^{-6}	1.40×10^{-3}	1.51×10^{-6}	6.88×10^{9}	1040[b]	…	…
HS $1.4M_\odot$ S	Quark core	1.68×10^{-2}	2.88×10^{-7}	7.96×10^{-13}	6.85×10^{-5}	1.01×10^{8}	1070	4.35×10^{8}	3690[a]
	Hadr. core		3.29×10^{-6}	1.25×10^{-3}	1.56×10^{-6}	3.61×10^{9}	394[c]	…	…
HS $2.0M_\odot$	Quark core	2.00×10^{-2}	5.25×10^{-6}	3.76×10^{-10}	2.34×10^{-2}	7.73×10^{6}	1080	4.77×10^{8}	6310[a]
	Hadr. core		5.24×10^{-6}	1.07×10^{-3}	1.32×10^{-6}	7.65×10^{9}	925[b]	…	…

[a]These values deviate significantly from the actual results due to the inappropriate approximation of constant radial profiles, whereas this idealization entirely fails for hadronic parts.
[b]The second minimum arises from the competition of the bulk viscosity damping in the quark and the hadronic shell.
[c]The second minimum arises from the competition of bulk and shear viscosity damping in the hadronic shell.

where the bulk viscosity is in general a function of the amplitude [17,18]. As has been noted before the strongly enhanced damping can provide a mechanism for the saturation of the r-mode as will be discussed elsewhere. Here we restrict ourselves to a study of the initial instability of small amplitude r-modes and in the subthermal regime the viscosity Eq. (8) is independent of the r-mode amplitude. In this case only the angular integral over the density fluctuation enters and it is useful to define the angular averaged form

$$\delta\Sigma(r) \equiv \frac{m+1}{2\alpha A R^2 \Omega^3}\sqrt{\frac{(m+1)^3(2m+3)}{4m}}\left(\int d\Omega |\delta\sigma|^2\right)^{1/2} \underset{\text{l.o.}}{\rightarrow} \left(\frac{r}{R}\right)^{m+1} + \delta\Phi_0, \tag{22}$$

which reduces to the second line to leading order in the Ω-expansion, where the angular integral in Eq. (21) is trivial due to the normalization of the spherical harmonics. The damping time in the subthermal regime is then given by

$$\frac{1}{\tau_B^<} = \frac{16m}{(2m+3)(m+1)^5\kappa}\frac{R^5\Omega^3}{\tilde{J}_m M}\mathcal{T}_m^<\left(\frac{T^\delta}{\kappa\Omega}\right), \tag{23}$$

where the dependence on all local quantities, like the equation of state, the weak rate, the density dependence of the particular star model and its r-mode profile is contained in the function

$$\mathcal{T}_m^<(b) \equiv \frac{b}{R^3}\int_{R_i}^{R_o} dr r^2 \frac{A^2C^2\tilde{\Gamma}}{1+\tilde{\Gamma}^2B^2b^2}(\delta\Sigma(r))^2, \tag{24}$$

depending on a single external parameter and which has to be determined numerically for a given star model. In the asymptotic limits the damping time simplifies to

$$\frac{1}{\tau_B^<} \underset{f\ll 1}{\longrightarrow} \frac{16m}{(2m+3)(m+1)^5\kappa^2}\frac{\Lambda_{\text{QCD}}^{9-\delta}\tilde{V}_m R^5\Omega^2 T^\delta}{\Lambda_{\text{EW}}^4\tilde{J}_m M} \tag{25}$$

$$\frac{1}{\tau_B^<} \underset{f\gg 1}{\longrightarrow} \frac{16m}{(2m+3)(m+1)^5}\frac{\Lambda_{\text{EW}}^4\Lambda_{\text{QCD}}^{\delta-1}\tilde{W}_m R^5\Omega^4}{\tilde{J}_m M T^\delta} \tag{26}$$

with the dimensionless constants

$$\tilde{V}_m \equiv \frac{\Lambda_{\text{EW}}^4}{R^3\Lambda_{\text{QCD}}^{9-\delta}}\int_{R_i}^{R_o} dr r^2 A^2C^2\tilde{\Gamma}(\delta\Sigma(r))^2 \tag{27}$$

$$\tilde{W}_m \equiv \frac{1}{R^3\Lambda_{\text{EW}}^4\Lambda_{\text{QCD}}^{\delta-1}}\int_{R_i}^{R_o} dr r^2 \frac{A^2C^2}{\tilde{\Gamma}B^2}(\delta\Sigma(r))^2. \tag{28}$$

Since the bulk viscosity originates from weak interactions here the second normalization scale Λ_{EW} is used with a generic value $\Lambda_{\text{EW}} = 100$ GeV. These normalization scales are only introduced to obtain dimensionless constants of order one and drop out of the final results for the damping times.

Finally, we want to stress that in these expressions for the r-mode time scales the complete local dependence on the star profile, the r-mode oscillation and the microscopic damping processes is contained in the few constant $\tilde{J}$, $\tilde{S}$, $\tilde{V}$ and $\tilde{W}$, but the dependence on the global parameters of the r-mode evolution [8] Ω and T is entirely explicit. These constants include, in particular, also the complete dependence on the nontrivial radial and angular dependence of the full next-to-leading order expression for the r-mode [3]. Since to our knowledge results for the bulk viscosity in the crust of neutron stars are not yet available, we neglect the damping of the crust in our numerical analysis. It has, however, been argued that the shear viscosity of the crust could be crucial [15] and a more detailed study of this issue is definitely desirable.

B. Results for the considered star models

Before we discuss the damping times for particular star models let us point out a few generic properties of the damping times that follow directly from the general expressions Eqs. (17), (19), and (23). The gravitational time scale is independent of temperature and decreases strongly with frequency. The shear viscosity damping time increases with temperature and is independent of frequency. Because of the resonant behavior of the bulk viscosity, the corresponding damping time decreases with temperature, has a minimum and increases again at large temperatures. Furthermore, it also decreases with frequency, but slower than the gravitational time scale.

A numeric solution requires the integration over the star profiles to obtain the constants $\tilde{J}$, $\tilde{S}$ and the function $\mathcal{T}^<$, respectively, the constants $\tilde{V}$ and $\tilde{W}$ describing its asymptotic behavior. The constants are given for the fundamental $m = 2$ r-mode of the various star models discussed in this work, and where applicable also for their different shells, in Table IV. For the bulk viscosity of a $1.4M_\odot$ neutron star we compute the APR result employing the proper susceptibilities for interacting matter, as well the result when the susceptibilities are evaluated in the idealized case of a hadronic gas, as has been done previously [39,41]. As can be seen the parameters in the interacting case are more than an order of magnitude larger, owing to the larger viscosity [17], which leads to a correspondingly smaller damping time. In the following we will consider only the proper interacting form unless otherwise noted.

In the left panel of Fig. 4 the numeric solution for the different time scales is shown as a function of temperature for $1.4M_\odot$ stars of the different classes considered here rotating at their Kepler frequency Ω_K. Shown are gravitational time scales (horizontal lines), the shear viscosity damping times (monotonically increasing curves) and bulk viscosity damping times (nonmonotonic curves). The solid lines denote the neutron star model, the dotted lines a strange star and the dashed and dot-dashed lines show hybrid star models with a small and large quark core,

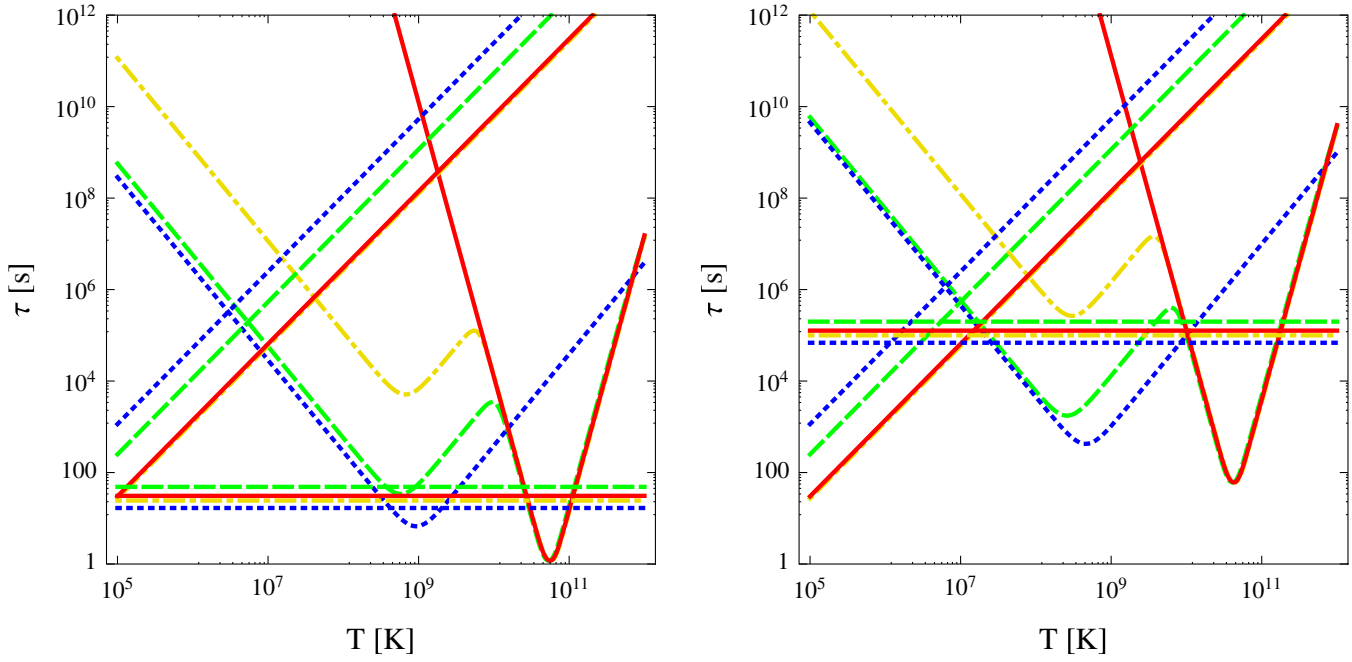

FIG. 4 (color online). Damping times of the different $1.4M_\odot$ star models discussed in this work. Shown are a hadronic star with modified Urca processes (solid), hybrid stars with a small (dot-dashed) and large (dashed) quark core as well as a strange star (dotted). The horizontal curves give the time scale τ_G associated to the growth of the mode due to gravitational wave emission. The monotonically increasing curves show the damping time τ_S due to shear viscosity and the nonmonotonic curves the damping time τ_B due to bulk viscosity. *Left panel:* Stars rotating at their Kepler frequency Ω_K. *Right panel:* Same for stars rotating at $\Omega_K/4$.

respectively. Whereas damping due to shear viscosity dominates for strange and hybrid stars for $T \lesssim 10^7$ K and for neutron stars even for $T \lesssim 10^9$ K, the bulk viscosity damping time of the neutron and the strange star feature the generic resonant form, where the minima are around 10^9 K and 10^{11} K, respectively, and the higher gradients in case of the neutron star arise from the higher power of δ (Table II). It is clear that as a function of the core size the family of hybrid curves interpolates continuously between the two uniform star models. Correspondingly, for hybrid stars the contribution of the quark core dominates at low temperature, whereas the hadronic shell dominates at higher temperatures, which leads to a curve with two minima. For all star models at Ω_K the gravitational time scale is the lowest over a range of temperatures.

The right panel of Fig. 4 shows the same plot at the lower frequency $\Omega_K/4$. As is clear from the general discussion the shear curves are unchanged whereas the gravitational curves and the bulk curves are shifted upwards compared to the left panel of Fig. 4. Since the gravitational time scale moves upwards faster than the bulk viscosity curve, the instability region shrinks from both sides as the frequency is lowered. For hybrid stars with a large quark core the gravitational time scale can move above the minimum of the bulk viscosity arising from the quark core as the frequency is lowered and the instability region is divided by a stability window. Yet, for a hybrid star with a sufficiently small quark core the minimum can move above the shear curve before the gravitational time scale can overtake it. In this case there would be no signature of the quark core and the instability regions of such a hybrid star and of the corresponding neutron star would look basically indistinguishable.[4] This is nearly the case for the small core hybrid star model denoted by the dot-dashed curve as will be discussed below.

V. R-MODE INSTABILITY REGIONS

The boundary of the instability region is given by the condition $|\tau_G| = |\tau_V|$, where τ_V is the viscous damping time. This reads in terms of the individual contributions

$$\frac{1}{\tau_G} + \sum_s \left(\frac{1}{\tau_S^{(s)}} + \frac{1}{\tau_B^{(s)}} \right) = 0. \tag{29}$$

Since at the boundary the time scale of the gravitational instability is identical to the viscous time scale, the r-mode amplitude neither increases nor decreases. If the viscous damping time is shorter modes induced by external perturbations will quickly be damped away, whereas in the opposite case they are unstable and will initially grow. As will be shown in a second article the increase in the

[4]The fact that the volume of the neutron shell is slightly smaller is not significant for the damping times that vary over many orders of magnitude, so that the dashed curves in Fig. 4 are invisible underneath the solid neutron star curves.

bulk viscosity at large amplitude can eventually saturate the r-mode, but here we will limit ourselves to the small amplitude regime and analyze the regions where small amplitude modes are unstable. In general Eq. (29) has no analytic solution and has to be solved numerically. However there are various limiting cases for which analytic solutions exist and we will study them below.

A. Analytic expressions

The boundary of the instability region Eq. (29) can generally not be found analytically due to the occurrence of several terms with nontrivial temperature and frequency dependencies. Since the viscous damping times vary extremely strongly with temperature and frequency (Fig. 4) in general there is over nearly the whole parameter space one component that clearly dominates the others in the sum. In such a case the equation can easily be solved analytically and yields analytic expressions for the different segments of the instability region. Although the numeric solution of Eq. (29) is straightforward, these analytic expressions reveal the general dependence on the various unknown model parameters entering the r-mode analysis and therefore provide a measure for the uncertainty of these results in a situation where most properties of dense strongly interacting are basically unknown. Here we give expressions for the fundamental $m = 2$ r-mode and the classes of stars discussed in this work and defer the general results to appendix B.

1. Low temperature boundary

As is clear from the analytic expressions for the damping times and confirmed by Fig. 4 at low temperatures shear viscosity damping dominates. Furthermore, in the case of hybrid stars the damping due to hadronic shear viscosity dominates over the quark core. Comparing it with the gravitational time scale yields

$$\Omega(T) \xrightarrow[T \ll T_{\min}]{} 1.12 \frac{\tilde{S}^{1/6} \Lambda_{\mathrm{QCD}}^{7/9}}{\tilde{J}^{1/3} G^{1/6} M^{1/3} R^{1/2}} T^{-(5/18)}, \quad \text{(NS and SS)},$$

where the irrational power arises from the Landau damping of the corresponding interactions that induce shear viscosity. Interestingly this expression depends only mildly on the constant $\tilde{S}$ that encodes the microscopic interaction. This segment of the boundary is important for old stars in binary systems that are spun up by accretion from a companion star and enter the instability region from below.

2. Minimum of the instability region

Since the shear viscosity damping time monotonically increases with temperature whereas the bulk viscosity damping time monotonically decreases at low temperature there is a minimum of the instability boundary given by $\tau_B = \tau_S$. Because of the nonlinear frequency dependence of the second order damping times an exact analytic solution is not possible. However, since these minima are located at frequencies far below the Kepler frequency it is according to Fig. 3 a very good approximation to use the leading order frequency connection $\kappa = \kappa_0$ in which case an analytic solution is possible. For neutron stars it reads

$$\Omega_{\min}^{(NS)} \approx 1.06 \frac{\Lambda_{\mathrm{QCD}}^{99/128} \tilde{S}^{9/64} \tilde{V}^{5/128}}{R^{49/128} \tilde{J}^{23/64} G^{23/128} M^{23/64} \Lambda_{\mathrm{EW}}^{5/32}} \tag{30}$$

$$T_{\min}^{(NS)} \approx 1.89 \frac{\tilde{S}^{3/32} \Lambda_{\mathrm{QCD}}^{1/64} \Lambda_{\mathrm{EW}}^{9/16} G^{3/64} \tilde{J}^{3/32} M^{3/32}}{\tilde{V}^{9/64} R^{27/64}}. \tag{31}$$

Note, the appearance of surprisingly low powers in these expressions. In particular, due to the arising $5/128$ power a change of $\tilde{V}$ by an order of magnitude results only in a mild deviation of the minimum frequency of less than 10%, and even a very drastic change by 3 orders of magnitude does not change the result by more than 30%. Whereas the viscosity constants Eqs. (27) and (28) can vary by many orders of magnitude for different classes of stars with different transport processes as can be seen from Table IV, they are generically of similar order of magnitude within a given class due to the identical parametric dependence on the microscopic physics. Recall, that the minimum of the instability region is of particular importance for the r-mode analysis since it determines to what frequency r-modes can spin down a star. It is needless to say that such an insensitivity of the minimum frequency on the microscopic physics is more than welcome in the present situation where there are still huge uncertainties on the underlying equation of state of dense matter and the transport coefficients of dense matter. This presents one of the main results of this article.

In the general case studied in appendix B the $(2m(\delta+\sigma)+2\delta)/\sigma$-th root of the bulk viscosity constants $\tilde{V}_m$ arises in the expression for the minimum frequency Eq. (B2). For short-range (Fermi liquid) interactions the shear viscosity exponent is generically $\sigma = 2$ whereas it reduces to $\sigma = 5/3$ when long-ranged, only Landau-damped (non-Fermi liquid) gauge interactions are present. Since the rate of the weak interactions vanishes in equilibrium and requires phase space both for initial and final state particles in general $\delta \geq 2$. A similar argument should hold for processes mediated by Goldstone bosons in color superconducting phases. Therefore the above root is for all multipoles and corresponding processes higher than 11 so that change of the viscosity constants $\tilde{V}_m$ by an order of magnitude still changes the minimum only by at most $\sim$20%, making it very insensitive to them. This extends the finding obtained in an explicit comparison of various different neutron star models in [6] to general forms of matter and damping processes. This insensitivity is particularly interesting since these constants contain the complete dependence on the detailed second order r-mode profiles, so that the minimum frequency is hardly affected by the second order effects. This

observation had already been made for the particular neutron star model studied in [3]. A similar statement holds for the dependence on the shear viscosity constants $\tilde{S}_m$, where the corresponding root is at least of 6th order reached in the limit $\delta \gg \sigma$. The temperature of the minimum is more sensitive to these constants, as likewise observed in [3,6], since it only involves the $(\sigma + \delta)$-th root.

Finally we give the explicit expression for the minimum frequency of strange stars with the general quark model equation of state Eq. (1). Here the parameter dependence of the quark matter viscosity coefficients given in Table II can be factored out according to

$$\tilde{\Gamma}^{(q)} \equiv \hat{\Gamma}\mu_q^5, \qquad \tilde{\eta}^{(q)} \equiv \hat{\eta}\alpha_s^{-5/3}\mu_q^{14/3}, \tag{32}$$

where $\hat{\Gamma}$ and $\hat{\eta}$ are pure constants, so that the minimum is located at

$$\Omega_{\min}^{(SS)} \approx 2.23\frac{\hat{\Gamma}^{5/56}\hat{\eta}^{3/28}m_s^{5/14}\mu_q^{43/56}}{G^{11/56}(1-c)^{5/28}\alpha_s^{5/28}R^{13/56}M^{11/28}} \tag{33}$$

$$T_{\min}^{(SS)} \approx 2.78\frac{\hat{\eta}^{3/14}G^{3/28}\mu_q^{1/28}(1-c)^{9/14}M^{3/14}}{\hat{\Gamma}^{9/28}\alpha_s^{5/14}m_s^{9/7}R^{27/28}}. \tag{34}$$

Assuming that Eq. (1) gives an estimate for the uncertainty in the unknown quark matter equation of state and estimating the uncertainty in the quadratic and quartic parameters m_s and $1 - c$ each by a factor of 2 and that in the strong coupling α_s generously by an order of magnitude, the minimum could vary here by roughly a factor of 2 owing to the uncertainty in the unknown microscopic dynamics. As noted before the quark model equation of state is also valid for color superconducting phases [31]. In this case the gap reduces the parameter m_s which would lower the minimum frequency and enlarge the instability region.

3. Intermediate boundary

Above the minimum the damping is dominated by the bulk viscosity and below its maximum it can be approximated by the asymptotic low temperature form Eq. (25). The semi-analytic result to next-to leading order in Ω is given in the appendix, but because of the small effect of the next-to-leading order corrections of the oscillation frequency on the instability regions, observed above, we can simply neglect these and obtain

$$\Omega(T)\xrightarrow[T\ll T_{\max}]{T\gg T_{\min}} 0.360\frac{\tilde{V}^{1/4}\Lambda_{\rm QCD}^{9/4}R^{1/4}}{\tilde{J}^{1/2}\Lambda_{\rm EW}G^{1/4}M^{1/2}}\cdot\begin{cases}\left(\frac{T}{\Lambda_{\rm QCD}}\right)^{3/2} & \text{(NS)}\\ \left(\frac{T}{\Lambda_{\rm QCD}}\right)^{1/2} & \text{(SS)}\end{cases}.$$

This part of the instability boundary is important for the spin-down of young compact stars since it determines where they hit the instability region during their initial fast cooling phase.

4. Maximum of the instability region for strange stars

Because of the resonant form of the bulk viscosity Eq. (8) whose maximum Eq. (10) translates into a minimum of the corresponding damping time, the instability region features a maximum if the corresponding frequency is below the Kepler frequency or otherwise splits into two parts. Since there is no analytic expression for the damping time in the vicinity of the maximum there is no general expression for the maximum. Yet, for hadronic matter the corresponding maximum frequency is usually above the Kepler frequency anyway so it is not relevant for physical applications. In contrast, for strange stars, where the maximum is generally below the Kepler frequency and important for the r-mode analysis, the density profile varies only mildly and can be approximated by a uniform density. In this case a general analytic expression for the maximum of the instability region is given in Eqs. (B5) and (B6), in appendix B and reduces using the susceptibilities in Table III to

$$\Omega_{\max}^{(SS)} \approx 0.434\frac{m_s^{4/3}R^{1/3}}{(1-c)^{1/3}G^{1/3}M^{2/3}} \tag{35}$$

$$T_{\max}^{(SS)} \approx 0.210\frac{(1-c)^{1/3}m_s^{2/3}R^{1/6}}{\hat{\Gamma}^{1/2}G^{1/6}\mu_q^{3/2}M^{1/3}}, \tag{36}$$

where the tiny second order corrections to the oscillation frequency, cf. Fig. 3, were neglected in this case. Note that analogous to the expression for the maximum of the viscosity of quark matter given in [17] the chemical potential drops out and therefore there is no ambiguity where to evaluate the susceptibilities in case the density distribution of the considered star model is not entirely constant. This gives for the dimensionless ratio

$$\frac{\Omega_{\max}^{(SS)}}{\Omega_K} \approx 1.03\frac{m_{150}^{4/3}R_{10}^{11/6}}{(1-c)^{1/3}M_{1.4}^{7/6}}, \tag{37}$$

where m_{150}, $M_{1.4}$ and R_{10} are the effective strange quark mass in units of 150 MeV, the stars mass in units of $1.4M_\odot$ and the radius in units of 10 km, respectively.

Whereas the dependence on the parameter c, which in the perturbative regime is positive and thereby increases the maximum frequency, is comparatively mild, the dependence on the effective strange quark mass is significant and can within the probable uncertainty region 100 MeV $\lesssim m_s \lesssim$ 200 MeV strongly change the position of the maximum frequency from values considerably below to values above the Kepler frequency. For superconducting matter the gap can reduce the effective parameter m_s. Whereas the maximum frequency of massive stars can be significantly lower, the radii of sufficiently massive strange stars do not vary much with mass along a mass-radius curve so that the

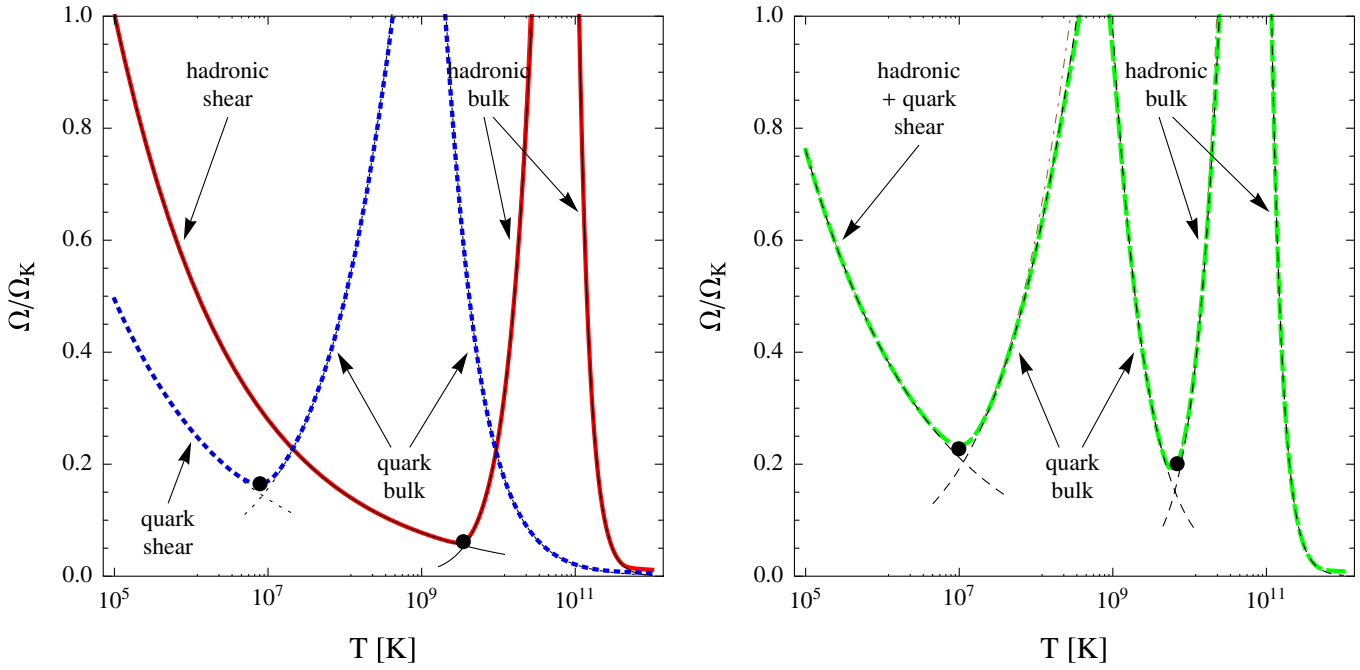

FIG. 5 (color online). Comparison of the numeric results for the instability region (thick lines) with the various approximate semi-analytic expressions (thin lines and blobs) presented in the text for the different classes of compacts stars. The dots present the results for the extrema and the thin lines which are valid away from the extrema represent the corresponding analytic results taking into account only the contribution from the dominant process and shell in the respective region. *Left panel:* Instability regions for the $1.4M_\odot$ neutron star (solid) and strange star model (dotted). *Right panel:* Same for the $1.4M_\odot$ hybrid star model. The thin dot-dashed curve on the right panel which deviates slightly close to the maximum is the leading order result without the frequency corrections in Fig. 3, whereas the corresponding curves are indistinguishable on the left panel. Note that here in the following where the ratio Ω/Ω_K is plotted this ratio is taken with the respective Kepler angular frequency for each star model, see Table I, so that the same value of Ω/Ω_K corresponds to a different value of Ω for different curves.

dependence on the radius is mild despite the arising high power. To judge the implicit dependence of the masses and radii on the equation of state it is useful to recall that the solution of the TOV equations for a uniform density star exhibits scaling with the bag constant R/R_0, $M/M_0 \sim \sqrt{B_0/B}$ [46]. Despite the uniform density approximation, the analytic result Eq. (37) for the maximum, given in Table IV, agrees nicely with the numeric results for the considered strange star models. The above expression can also be applied to the corresponding analysis of Jaikumar, *et al.* [7]. Using their lower strange quark mass $m_s = 100$ MeV as well as their slightly smaller radius and taking into account that these authors erroneously used the angular velocity in the inertial frame to evaluate the bulk viscosity yields $\Omega^{(SS)}_{\max}/\Omega_K \approx 0.47$ in very good agreement with the plot of the exclusion region shown in their Fig. 4. When employing the proper angular velocity in the rotating frame, Eq. (37), gives instead the corrected result $\Omega^{(SS)}_{\max}/\Omega_K \approx 0.59$.

The analytic results in appendix B to some extent also apply to the maxima of the instability regions of hybrid stars but in this case the agreement is less precise since the density profile of their quark core features a more pronounced radial dependence.

5. High temperature boundary

For completeness we also give the high temperature part of the boundary.

$$\Omega(T) \xrightarrow[T \gg T_{\max}]{} 8.66 \times 10^{-2} \frac{\tilde{W}^{1/2} \Lambda_{\rm EW}^2 R^{1/2}}{\tilde{J} \Lambda_{\rm QCD}^{1/2} G^{1/2} M} \cdot \begin{cases} \left(\frac{\Lambda_{\rm QCD}}{T}\right)^3 & \text{(NS)} \\ \frac{\Lambda_{\rm QCD}}{T} & \text{(SS)} \end{cases}.$$

Because of the resonant behavior of the bulk viscosity which decreases again at large temperatures, the r-mode is unstable for all forms of matter at large temperatures above the corresponding boundary of the shell with the largest resonance temperature Eq. (10). This part could be less relevant for the r-mode evolution since stars cool very fast initially and could leave this region before the r-mode can develop.

6. General properties of the analytic analysis

Finally let us note a few generic properties of these analytic results. Since the mass appears in the denominator in all these expressions, an increase of the mass of the star increases the instability region and moves it uniformly downward and slightly to the right in a $T - \Omega$ plot. The dependence on the radius is less uniform, but in general

these expressions are less sensitive to the radius than to the mass of the star. Furthermore for a given equation of state the radius of a star varies very little for masses of 1 to $2M_\odot$. As already noted, the dependence of the minima of the instability region on the viscosity parameters is extremely mild. Because of the arising small powers $O(1/10)$ even a large variation of the viscosity parameters by 3 orders of magnitude within the set of possible equations of state for a given class of stars, like e.g. pure neutron stars would not change the minimum by more than a factor of 2. In contrast the dependence of the maxima on the viscosity parameters is far more pronounced and as discussed above changes by more than a factor of 2 are here easily possible.

B. Numeric results

Let us now discuss the numeric results for the exclusion regions and compare them to the semi-analytic expressions obtained in the last section in order to assess the quality of the latter. Figure 5 compares the expressions for particular segments of the instability region and for the extrema to the numeric solution. The left panel shows the results for a standard $1.4M_\odot$ neutron star model (solid) and a corresponding strange star model (dotted). The thick curves show the numeric results and the thin curves the analytic approximations and the dots denote the minima. Since we neglect the contribution from the neutron star crust there is only a single shell in each case. As can be seen, except for the regions around the extrema, the analytic expressions for the different segments approximate the boundary of the instability region extremely well and are mostly hidden underneath the numeric curves. Yet, the extrema are in turn well described by the corresponding analytic expressions. As noted in [4,7,11], due to the resonant form of the bulk viscosity there is a stability window around 10^9 K where strange stars are not unstable against r-modes up to large frequencies. For the considered strange star model the maximum of the instability region is above the Kepler frequency so that two separate regions appear, but as discussed before the position of the maximum depends on the particular microscopic parameters. Because of the same qualitative resonant structure of the bulk viscosity there is also a second instability region at high temperatures $\gtrsim 10^{11}$ K for neutron stars that has previously been neglected due to the employed low temperature approximation to the hadronic bulk viscosity [39,41]. Although the r-mode is initially unstable the naive expectation is that this should be irrelevant for the spin-down evolution since the star cools extremely fast at such high temperatures and might leave this region before r-modes can develop. Yet, since the interior of the star is initially opaque to neutrinos and the cooling is delayed this is not entirely clear and requires further study.

On the right panel of Fig. 5 the comparison for the $1.4M_\odot$ hybrid star model is shown. Here there are contributions from the different layers, but strikingly the analytic approximation works even in this more complicated case. This plot shows nicely the generic structure of the boundary of the instability region, discussed in the previous subsection, when several shells are present that feature qualitatively different damping mechanisms. Around its resonant temperature the bulk viscosity damping mechanism of a given shell in general clearly dominates over those of the other shells. If the resonant temperatures of the different bulk viscosities are sufficiently separated there are several maxima, that define corresponding stability windows. Below each of these maxima there is a minimum where a dominant mechanism is replaced by the next. However, in case two resonant temperatures are too close or a shell is too small to have a sizable impact, individual stability windows can be fully or partly washed out. We discuss such cases below.

Figure 6 shows the exclusion region for the standard $1.4M_\odot$ neutron star model compared to approximations used previously in the literature. The solid curve shows our new result with shear viscosity due to the dominant Landau-damped lepton scattering [43] and bulk viscosity due to modified Urca processes based on susceptibilities

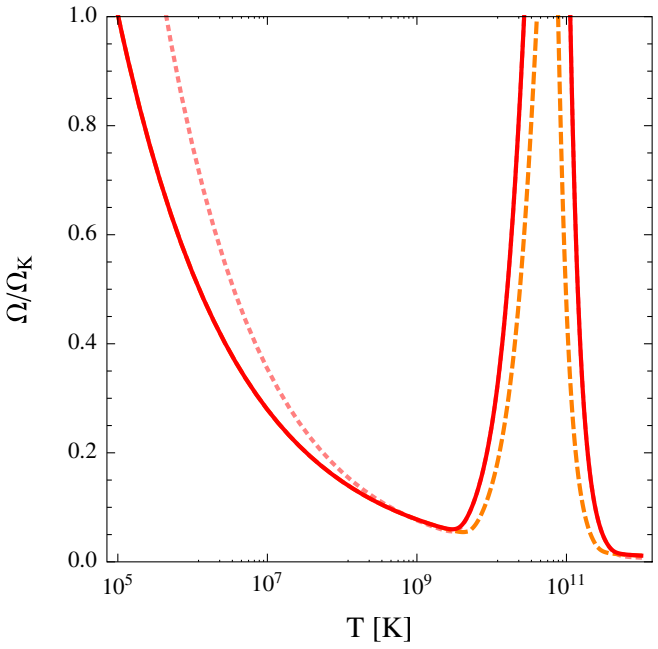

FIG. 6 (color online). Modification of the instability region of a $1.4M_\odot$ neutron star due to improved approximations for the microscopic transport properties. The solid curve shows the standard neutron star model with shear viscosity due to the dominant Landau-damped lepton scattering and bulk viscosity based on the proper susceptibilities for interacting matter (as all other neutron star results in this work). The dashed curve shows the result when using the fit given in [41] to the density data $\lesssim n_0$ for the shear viscosity from hadron-hadron-scattering obtained in [42]. The dotted line shows the result when employing the previously used expression neglecting interactions to the susceptibilities contributing to the bulk viscosity [39,41].

for interacting matter [17]. The dotted curve shows the exclusion region when using the result for the shear viscosity from the fit in [41] to the standard low density ($\lesssim n_0$) data from hadron-hadron-scattering given in [42]. Extrapolating this fit to high densities relevant for neutron stars overestimates the viscosity compared to its actual, subleading size [43], leading to the smaller exclusion region. The dashed curve shows the result when employing the previously used expression for the bulk viscosity [39,41] which employs susceptibilities in the approximation of an ideal hadron gas, see Table III. It is again the insensitivity to the viscosity parameter $\tilde{V}$ discussed in the previous subsection that is responsible for the fact that these corrections, which change the damping time by more than an order of magnitude, have only such a mild effect on the exclusion region and the minimum Eq. (30). It is interesting that the effect of the interactions is opposite to that of the 2nd order Ω corrections [3]. The combined curve formed by the dotted and the dashed segment is the exclusion region that had previously been studied in the literature. As can be seen the combined effect of both corrections is to move the instability region to lower temperatures so that it extends to roughly 10^5 K. This is relevant for old stars at low temperatures that are spun up by accretion since the r-mode becomes unstable already at lower frequencies.

The left panel of Fig. 7 compares the instability regions of the different $1.4M_\odot$ star models considered here and also includes the analytic results for the extrema. The minima in these plots corresponds to the maxima where two damping mechanisms cross in Fig. 4 whereas the maxima in Fig. 7 correspond to the minima in Fig. 4. As can be seen the instability regions of the hybrid stars interpolate between the neutron star and the strange star curve as the size of the quark core increases, even though all these curves are based on rather different equations of state distinguished by the interaction parameter c, see Table I. The right panel of Fig. 7 shows the instability regions for the $2M_\odot$ models discussed in this work. As has already been observed as a generic feature of the analytic analysis, the r-mode instability in heavy stars is enhanced and the boundary of the instability region moves slightly to lower frequencies. As predicted by the mass dependences of the analytic expressions this is most pronounced in the vicinity of the maxima and milder in the vicinity of the minima. The approximate analytic results for the maxima deviate slightly from the maxima of the numerical curves. The reason for this is that the uniform density approximation is not justified in this case due to the strong radial dependence of the density profiles, see Fig. 2.

Figure 8 shows the instability region for an ultraheavy neutron star $M \approx 2.2M_\odot$ denoted by the solid curve. Here, the instability region has grown to the point that the lower and the upper part are about to merge. For this star the densities that are reached are high enough that direct Urca processes are kinematically allowed within an inner core with radius of roughly $R/2$. The enhanced damping due to direct Urca bulk viscosity in the inner core leads to a notch

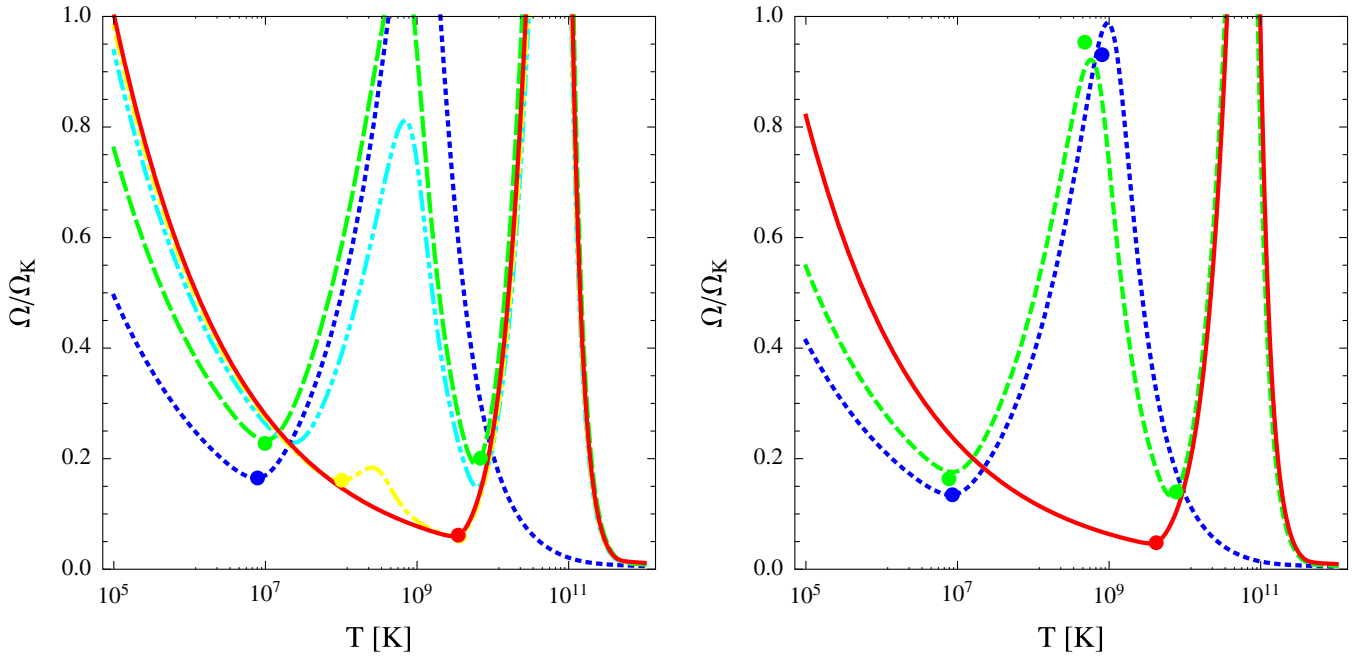

FIG. 7 (color online). Instability regions for the different star models considered in this work. Shown are neutron star models with APR equation of state (solid), hybrid stars with a small (dot-dashed), a medium (dot-dot-dashed) and a large quark matter core (dashed) and strange star models (dotted) with an ideal gas equation of state. The blobs show again the analytic estimates for the extrema. *Left panel:* $1.4M_\odot$ stars. *Right panel:* $2M_\odot$ stars, for which for the considered equations of state stars with smaller quark cores could not be found.

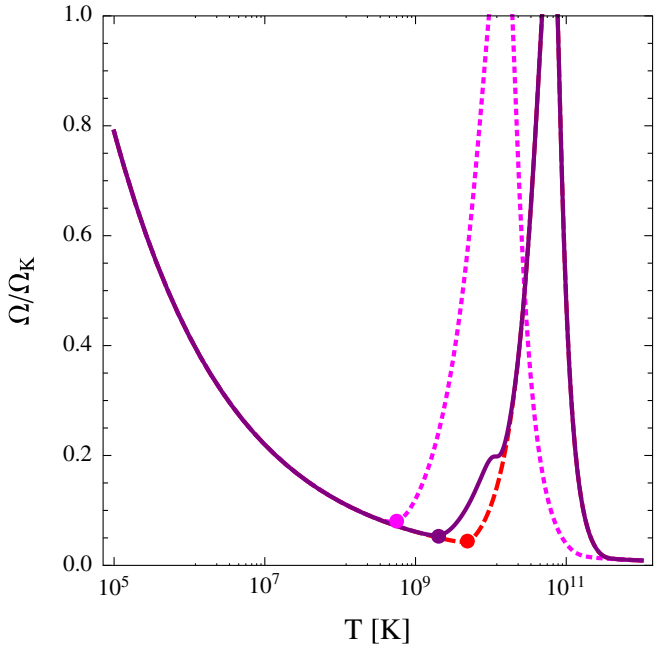

FIG. 8 (color online). The instability region with direct Urca interactions is shown for the $2.21M_\odot$ maximum mass neutron star model (solid curve), where direct Urca processes are allowed in the inner core but only modified Urca processes in the layer surrounding it. For comparison the instability region is shown when direct Urca reactions are artificially suppressed (dashed curve) as well as when they are artificially allowed in the entire hadronic core (dotted curve).

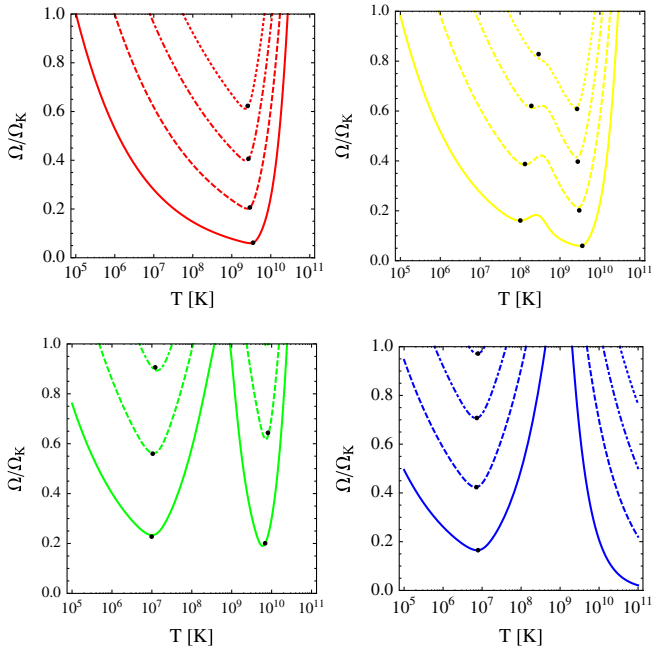

FIG. 9 (color online). Instability regions for the first four multipole r-modes ($m = 2$ to 5) of the different $1.4M_\odot$ star models (top, left: neutron star; top, right: hybrid star, small quark core; bottom, left: hybrid star, large quark core; bottom right: strange star). The minima from Eqs. (B2) and (B3), the second minima of the large core hybrid star from Eqs. (B8) and (B9) and the maxima from Eqs. (B5) and (B6) are denoted by the dots. For higher multipoles the size of the instability regions decreases and they move to higher rotation frequencies, so that all modes with $m \geq 7$ are entirely stable in the physical range of frequencies. In particular in the cases of neutron and hybrid stars the right boundaries of the instability regions of the higher multipoles are very close to the fundamental $m = 2$ mode, so that several modes can easily be excited if the evolution significantly enters the fundamental instability region.

at the right side of the instability region, as also found in [47]. Yet, the modification is rather mild in this case: the dashed curve shows the same star model when direct Urca processes are artificially suppressed. In the opposite extreme when direct Urca processes are artificially allowed in the entire core, shown by the dotted curve, the enhanced damping does lead to a significant change of the instability region. Moreover, the frequency of the minimum of the instability region increases. Because of the resonant form of the bulk viscosity, however, the instability region does not uniformly shrink over the whole temperature range where bulk viscosity dominates, but the stability window moves to lower temperatures leaving the r-mode unstable at higher temperatures where it is otherwise stable in the presence of modified Urca processes. The temperature scales of the corresponding stability windows agree with the temperature scales of the resonant maximum of the bulk viscosity, see [17]. Direct Urca processes are very sensitive to the proton fraction of dense matter. Whereas the required fraction is roughly 14% in the case of the APR equation of state, reached at relatively high densities $\gtrsim 5n_0$, this could be different for other equations of state. In a case where the direct Urca core is larger but a modified Urca shell is still present so that both of them have a sizeable volume fraction, their combined damping could lead to a larger stability window, yet still at parametrically larger temperatures than the stability window of strange stars.

Figure 9 shows the result for the higher multipoles for the different $1.4M_\odot$ star models. As can be seen, the right boundaries of the instability regions for the higher multipoles are extremely close to the boundary of the fundamental $m = 2$ mode. Correspondingly these modes could easily be excited once the evolution of a star enters the instability region. Each mode that is triggered would lead to a further enhancement of the spin-down of the star and could change the evolution. This could be particularly relevant for young neutron stars that enter the instability region at high temperatures when the cooling is still fast but there are no strong reheating mechanisms which could prevent the star from substantially penetrating the instability region.

Figure 10 finally compares our numeric results to astrophysical data. Although the rotation frequencies of pulsars are known to high accuracy, the relevant core temperatures are not known for most pulsars and involve large uncertainties even for those stars where estimates are available.

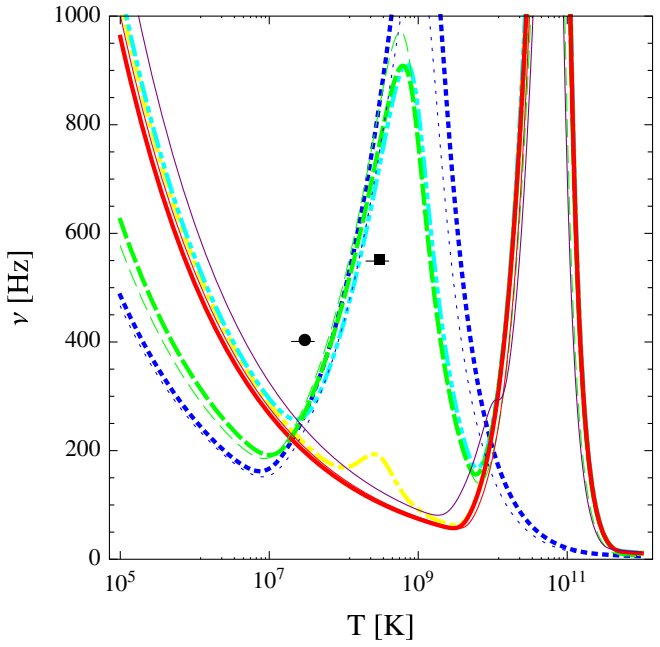

FIG. 10 (color online). Comparison of the instability regions in absolute frequencies for the different star models considered in this work with the two low mass X-ray binaries Aql X-1 (filled square) and SAX J1808.4-3658 (open circle). The horizontal bar gives a partial measure for the error within the model computations which should be larger due to uncontrolled assumptions that are not considered in its size.

The reason is that the temperature of the surface is indirectly inferred from the data and it is necessary to abstract from it the core temperature via models. Such an analysis has been performed for two low mass X-ray binary systems Aql X-1 and SAX J1808.4-3658 [48], where the pulsars accrete matter from companion stars. The horizontal lines give an optimistic estimate for the uncertainty of the temperature. As can be seen these data points are well within the instability region of neutron stars. This holds, in particular, for the faster one of the two pulsars, Aql X-1, which is right in the middle. Our analysis shows this statement cannot be undermined by the unknown equation of state. So if r-modes would spin down stars so fast that the stars would leave the unstable region on time scales short compared to astrophysical ones these stars could not be pure neutron stars and would require some form of enhanced damping. Yet, in the case of strange stars and hybrid stars with a sufficiently large quark core, the data points are close to the boundary of the corresponding stability window and would be compatible in such a scenario.[5] As our results show, hybrid stars with a small quark core or neutron stars with enhanced hadronic direct Urca damping, in contrast, would not be sufficient.

[5]A potential problem with such an explanation of the data would be the observation of a very fast and at the same time very cold pulsar, since, after the accretion stops, stars within the stability window would reenter the instability region due to cooling and correspondingly would have to spin down to a fraction of their Kepler frequency.

VI. CONCLUSIONS

Using general expressions for the viscosities of dense matter we have derived semi-analytic results for the damping times of small amplitude r-mode oscillations and the boundary of the instability region. Our results show that the boundary of the instability region and, in particular, its minimum, which determines to what extent r-modes can spin down a fast star, are extremely insensitive to the quantitative details of the microscopic interactions that induce viscous damping. However, the instability regions can nevertheless effectively discriminate between qualitatively different classes of stars. In particular strange stars and hybrid stars with sufficiently large quark cores feature a stability window that cannot be reproduced with standard neutron stars without some admixture of exotic matter that provides enhanced damping. We find that the presence of some form of exotic matter does not automatically lead to a stability window since the instability region of hybrid stars with a sufficiently small quark core is almost indistinguishable from that of a neutron star. Similarly, the presence of neutron matter with direct Urca interactions will in most cases not considerably change the instability region. However, due to the demonstrated insensitivity of the instability regions to quantitative microscopic details, the clear determination of a very fast pulsar with $\Omega > 300$ Hz in the temperature range around 10^9 K could provide a convincing signature for some exotic form of matter. What remains to be shown in order to transform this into a strict signature is that the crust does not dominate the damping, and that r-modes do not saturate at amplitudes that are so small that the spin-down takes billions of years in which case the instability region would not really present a no-go area. The second point requires a thorough understanding of the dynamical evolution of compact stars and a step towards this goal is taken in a companion paper [16] where we show that the large amplitude behavior of the bulk viscosity can saturate r-modes at amplitudes that are large enough for a fast spin-down.

ACKNOWLEDGMENTS

We thank N. Andersson, G. Comer, B. Haskell, P. Jaikumar, A. Reisenegger and A. Steiner for helpful discussions. This research was supported in part by the Offices of Nuclear Physics and High Energy Physics of the U.S. Department of Energy under Contracts Nos. DE-FG02-91ER40628 and DE-FG02-05ER41375.

APPENDIX A: ANALYTIC FORM FOR THE R-MODE PROFILE OF CONSTANT DENSITY STARS

In this appendix we give an analytic solution for the density fluctuation profile of the r-mode to leading order in

Ω for a star of constant density. The part of the leading order density fluctuation Eq. (6) that is generally not analytic is given by the change in the gravitational potential $\delta\Phi_0$ whose radial part $\delta\Phi_0(r)$ is defined by

$$\delta\Phi_0(\vec{r}) = \sqrt{\frac{m}{\pi(m+1)^3(2m+1)!}}\alpha\,\delta\Phi_0(r)P^m_{m+1}(\cos\theta)e^{im\varphi}.$$

It fulfills the differential equation [3]

$$\frac{d^2\delta\Phi_0}{dr^2} + \frac{2}{r}\frac{d\delta\Phi_0}{dr} + \left(4\pi G\rho\frac{d\rho}{dp} - \frac{(m+1)(m+2)}{r^2}\right)\delta\Phi_0 = -4\pi G\rho\frac{d\rho}{dp}\left(\frac{r}{R}\right)^{m+1}$$

with boundary conditions $\delta\Phi_0(0) = 0$ and

$$\left.\frac{d\delta\Phi_0(r)}{dr}\right|_{r=R} = -\left(\frac{1}{2} + \sqrt{\frac{1}{4} + (m+1)(m+2)}\right)\frac{\delta\Phi_0(R)}{R}.$$

Here we specialize to the fundamental $m = 2$ r-mode where an analytic solution is possible for the idealized case $\rho = \text{const}$ and $d\rho/dp = \text{const}$ which is approximately realized for strange stars. The solution obtained with a computer algebra system reads

$$\delta\Phi_0(r) = -\frac{r^3}{R^3} + \frac{7LR^2((r^3 - 15L^2r)\cos(\frac{r}{L}) + 3L(5L^2 - 2r^2)\sin(\frac{r}{L}))}{r^4((3L^2 - R^2)\sin(\frac{R}{L}) - 3LR\cos(\frac{R}{L}))}$$

in terms of the intrinsic length scale

$$L \equiv \frac{1}{\sqrt{4\pi G\rho\frac{\delta\rho}{\delta p}}}.$$

Unfortunately the above expression is rather ill behaved due to strong cancellations and not suitable for a direct evaluation. However, employing the series representations of the trigonometric functions it is possible to transform it into an alternative form

$$\delta\Phi_0(r) = g\left(\frac{r}{L}, \frac{R}{L}\right)\frac{r^3}{R^3}$$

in terms of hypergeometric functions

$$g(x,y) \equiv \frac{{}_0F_2(\frac{1}{2}, \frac{7}{2} + 1; -\frac{x^2}{8})}{{}_0F_2(\frac{1}{2}, \frac{5}{2} + 1; -\frac{y^2}{8})} - 1 \approx -\frac{x^2}{18} + \frac{y^2}{14} + \cdots$$

Correspondingly, $|g| < 0.07$ over the entire parameter range so that in view of the large uncertainties inherent in an r-mode analysis the gravitational potential term in Eq. (6) can be neglected leaving a simple analytic expression for the r-mode profile of strange stars with approximately constant density.

APPENDIX B: GENERAL SEMI-ANALYTIC EXPRESSIONS FOR THE BOUNDARY OF THE INSTABILITY REGION

In this appendix we give the general semi-analytic expressions for the boundary of the instability region that are valid for arbitrary multipoles and can be applied to stars involving several shells. The only nonanalytic input in these expressions enters via the radial integral constants $\tilde{J}$, $\tilde{S}$, $\tilde{V}$ and $\tilde{W}$ arising in the gravitational time scale, the shear viscosity time scale as well as the low and high temperature limit of the bulk viscosity time scale. In general these constants, which are given for the star models discussed in this work and the normalization scales $\Lambda_{\rm QCD} = 1$ GeV and $\Lambda_{\rm EW} = 100$ GeV in Table IV, have to be computed numerically. However, since the dependence of many of the following results on these constants is surprisingly weak, these expressions are often essentially analytic.

On the low temperature side of the instability region the shear viscosity dominates and neglecting the bulk viscosity yields the analytic result for the boundary in this region

$$\Omega(T) \xrightarrow[T \ll T_{\rm min}]{} \left(\frac{(2m+1)((2m+1)!!)^2(m+1)^{2m+2}}{32\pi(m+2)^{2m+2}(m-1)^{2m-1}}\frac{\tilde{S}_m\Lambda^{3+\sigma}_{\rm QCD}}{\tilde{J}^2_m GM^2R^{2m-1}T^\sigma}\right)^{(1/(2m+2))}. \tag{B1}$$

In the case of a hybrid star with two or more distinct shells one of them generally dominates and the above expression applies using only the contribution $\tilde{S}$ of the dominant shell as well as the corresponding exponent σ. The dominant contribution to the inverse shear viscosity damping time arises from the hadronic shell. Since the shear damping time increases monotonically with temperature whereas the bulk viscosity decreases in this regime monotonically, the minimum of the instability region is taken at the temperature where $\tau_S = \tau_B$. The minimum frequency is then obtained from $1/\tau_G + 2/\tau_B = 0$ and taking into account that at low frequency $\kappa \approx \kappa_0$ it yields

$$\Omega_{\rm min} \approx \left(\left(\frac{m(m+1)^{2m-1}((2m+1)!!)^2}{4\pi(2m+3)(m+2)^{2m+2}(m-1)^{2m}}\right)^\sigma\left(\frac{((2m+1)!!)^2(2m+1)(m+1)^{2m+2}}{16\pi(m-1)^{2m-1}(m+2)^{2m+2}}\right)^\delta \times \frac{\tilde{V}^\sigma_m\tilde{S}^\delta_m\Lambda^{3\delta+9\sigma}_{\rm QCD}}{\tilde{J}^{2(\delta+\sigma)}_m\Lambda^{4\sigma}_{\rm EW}G^{\delta+\sigma}R^{2m(\delta+\sigma)-\delta-5\sigma}M^{2(\delta+\sigma)}}\right)^{(1/(2m(\delta+\sigma)+2\delta))}, \tag{B2}$$

whereas the corresponding minimum temperature is

$$T_{\min} \approx \left(\frac{(2m+3)(2m+1)(m+1)^3(m-1)}{4m}\,\frac{\tilde{S}_m \Lambda_{\rm EW}^4 \Lambda_{\rm QCD}^{\delta+\sigma-6}}{\tilde{V}_m R^4}\right)^{(1/(\delta+\sigma))} \Omega_{\min}^{-(2/(\delta+\sigma))}. \tag{B3}$$

Above the minimum the bulk viscosity dominates and increases until it reaches a maximum. Within a temperature range in between these two extrema shear viscosity can be neglected and the low temperature approximation to the bulk viscosity can be applied. In the general case the equation $1/\tau_B + 1/\tau_G = 0$ for the boundary cannot be solved analytically as a function of T due to the nonlinear second order terms in Ω. However, it is possible to solve the equation analytically as a function of Ω which provides an equally valid parameterization of the segment in between the two extrema

$$T(\Omega) \xrightarrow[\Omega \ll \Omega_{\max}]{\Omega_{\min} \ll \Omega} \left(\frac{2\pi(2m+3)(m+2)^{2m+2}(m-1)^{2m}\kappa^2}{m(m+1)^{2m-3}((2m+1)!!)^2}\,\frac{\tilde{J}_m^2 \Lambda_{\rm EW}^4 G M^2 \Omega^{2m}}{\tilde{V}_m \Lambda_{\rm QCD}^{9-\delta} R^{5-2m}}\right)^{1/\delta}. \tag{B4}$$

Since there is no analytic expression for the bulk viscosity around the maximum only for the special case of constant density stars a result is possible. In this case the maximum frequency is

$$\Omega_{\max} \xrightarrow[\text{density}]{\text{uniform}} \left(\frac{2\pi m(m+1)^{2m-2}(2m+3)((2m+1)!!)^2}{9(2m+5)(m+2)^{2m+2}(m-1)^{2m}}\,\frac{\bar{A}^2\bar{C}^2(R_o^3 - R_i^3)}{G\bar{B}M^2R^{2m-2}}\right)^{(1/(2m-1))}, \tag{B5}$$

where R_i and R_o are the inner and outer radii of the dominant shell (0 and R for a homogeneous star) and bars denote average quantities over the shell in case the density is only approximately constant. The corresponding maximum temperature is

$$T_{\max} \xrightarrow[\text{density}]{\text{uniform}} \left(\frac{2\Omega_{\max}}{(m+1)\bar{\tilde{\Gamma}}\,\bar{B}}\right)^{1/\delta}. \tag{B6}$$

In general the constant density approximation is only valid for quark matter and the corresponding results in this case are given in the main text. However, for neutron stars the corresponding maximum is in general above the Kepler frequency anyway and therefore not physically interesting. Far above the temperature where the maximum is located the high temperature approximation to the bulk viscosity is valid and the boundary $1/\tau_B + 1/\tau_G = 0$ condition yields here

$$\Omega(T) \xrightarrow[T \gg T_{\max}]{} \left(\frac{m(m+1)^{2m-3}((2m+1)!!)^2}{2\pi(2m+3)(m+2)^{2m+2}(m-1)^{2m}} \cdot \frac{\tilde{W}_m \Lambda_{\rm EW}^4 \Lambda_{\rm QCD}^{\delta-1} R^{5-2m}}{\tilde{J}_m^2 G M^2 T^{\delta}}\right)^{(1/(2m-2))}. \tag{B7}$$

For homogeneous stars the present approximations cover nearly the entire boundary of the instability region. If the star has more than one layer, there may be a second minimum. Depending on the size of the layers here it can be either the bulk viscosity of the second layer that equals the dominant shear viscosity at the minimum, in which case the above expressions hold, or the bulk viscosities of the different layers are identical $\tau_B^{(i)} = \tau_B^{(o)}$ which yields analogously

$$\begin{aligned}\Omega_{\min}^{(B)} = \Bigg(\Bigg(&\frac{m(m+1)^{2m-3}((2m+1)!!)^2}{\pi(2m+3)(m-1)^{2m}(m+2)^{2m+2}}\Bigg)^{\delta^{(o)}+\delta^{(i)}} \cdot \left(\frac{m+1}{2}\right)^{2\delta^{(i)}} \\ &\times \frac{\Lambda_{\rm QCD}^{9\delta^{(i)}-\delta^{(o)}} (\tilde{V}_m^{(o)})^{\delta^{(i)}} (\tilde{W}_m^{(i)})^{\delta^{(o)}}}{\Lambda_{\rm EW}^{4(\delta^{(i)}-\delta^{(o)})} G^{(\delta^{(o)}+\delta^{(i)})} \tilde{J}_m^{2(\delta^{(o)}+\delta^{(i)})}} \cdot \frac{R^{(5-2m)(\delta^{(o)}+\delta^{(i)})}}{M^{2(\delta^{(o)}+\delta^{(i)})}}\Bigg)^{(1/(2m(\delta^{(o)}+\delta^{(i)})-2\delta^{(o)}))}\end{aligned} \tag{B8}$$

and the corresponding temperature is

$$T_{\min}^{(B)} = \left(\frac{4}{(m+1)^2} \cdot \frac{W_m^{(i)} \Lambda_{\rm EW}^8 \Lambda_{\rm QCD}^{\delta^{(o)}+\delta^{(i)}-10}}{V_m^{(o)}}\right)^{(1/(\delta^{(o)}+\delta^{(i)}))} (\Omega_{\min}^{(B)})^{(2/(\delta^{(o)}+\delta^{(i)}))}. \tag{B9}$$

[1] M. G. Alford, A. Schmitt, K. Rajagopal, and T. Schafer, Rev. Mod. Phys. **80**, 1455 (2008).
[2] J. Papaloizou and J. E. Pringle, Mon. Not. R. Astron. Soc. **182**, 423 (1978).
[3] L. Lindblom, G. Mendell, and B. J. Owen, Phys. Rev. D **60**, 064006 (1999).
[4] N. Andersson and K. D. Kokkotas, Int. J. Mod. Phys. D **10**, 381 (2001).

[5] N. Andersson, Astrophys. J. **502**, 708 (1998).
[6] L. Lindblom, B. J. Owen, and S. M. Morsink, Phys. Rev. Lett. **80**, 4843 (1998).
[7] P. Jaikumar, G. Rupak, and A. W. Steiner, Phys. Rev. D **78**, 123007 (2008).
[8] B. J. Owen *et al.*, Phys. Rev. D **58**, 084020 (1998).
[9] N. Andersson, K. D. Kokkotas, and B. F. Schutz, Astrophys. J. **510**, 846 (1999).
[10] C. D. Ott, A. Burrows, T. A. Thompson, E. Livne, and R. Walder, Astrophys. J. Suppl. Ser. **164**, 130 (2006).
[11] J. Madsen, Phys. Rev. Lett. **85**, 10 (2000).
[12] L. Lindblom and B. J. Owen, Phys. Rev. D **65**, 063006 (2002).
[13] P. Demorest, T. Pennucci, S. Ransom, M. Roberts, and J. Hessels, Nature (London) **467**, 1081 (2010).
[14] F. Ozel, D. Psaltis, S. Ransom, P. Demorest, and M. Alford, Astrophys. J. Lett. **724**, L199 (2010).
[15] L. Bildsten and G. Ushomirsky, Astrophys. J. Lett. **529**, L33 (2000).
[16] M. G. Alford, S. Mahmoodifar, and K. Schwenzer, arXiv:1103.3521.
[17] M. G. Alford, S. Mahmoodifar, and K. Schwenzer, J. Phys. G **37**, 125202 (2010).
[18] J. Madsen, Phys. Rev. D **46**, 3290 (1992).
[19] A. Reisenegger and A. A. Bonacic, arXiv:astro-ph/0303454.
[20] A. A. Bonacic, Master thesis, Universidad Catolica de Chile, 2003.
[21] R. C. Tolman, Phys. Rev. **55**, 364 (1939).
[22] P. Haensel, K. P. Levenfish, and D. G. Yakovlev, Astron. Astrophys. **357**, 1157 (2000).
[23] P. Haensel, K. P. Levenfish, and D. G. Yakovlev, Astron. Astrophys. **372**, 130 (2001).
[24] B. Haskell, N. Andersson, and A. Passamonti, Mon. Not. R. Astron. Soc. **397**, 1464 (2009).
[25] A. Akmal, V. R. Pandharipande, and D. G. Ravenhall, Phys. Rev. C **58**, 1804 (1998).
[26] G. Baym, C. Pethick, and P. Sutherland, Astrophys. J. **170**, 299 (1971).
[27] J. W. Negele and D. Vautherin, Nucl. Phys. **A207**, 298 (1973).
[28] E. S. Fraga, R. D. Pisarski, and J. Schaffner-Bielich, Phys. Rev. D **63**, 121702 (2001).
[29] E. S. Fraga and P. Romatschke, Phys. Rev. D **71**, 105014 (2005).
[30] A. Kurkela, P. Romatschke, and A. Vuorinen, Phys. Rev. D **81**, 105021 (2010).
[31] M. Alford, M. Braby, M. W. Paris, and S. Reddy, Astrophys. J. **629**, 969 (2005).
[32] E. Witten, Phys. Rev. D **30**, 272 (1984).
[33] K. H. Lockitch, N. Andersson, and J. L. Friedman, Phys. Rev. D **63**, 024019 (2000).
[34] K. H. Lockitch, J. L. Friedman, and N. Andersson, Phys. Rev. D **68**, 124010 (2003).
[35] J. Ruoff and K. D. Kokkotas, Mon. Not. R. Astron. Soc. **330**, 1027 (2002).
[36] P. Haensel and R. Schaeffer, Phys. Rev. D **45**, 4708 (1992).
[37] A. Reisenegger, Astrophys. J. **442**, 749 (1995).
[38] B. L. Friman and O. V. Maxwell, Astrophys. J. **232**, 541 (1979).
[39] R. F. Sawyer, Phys. Rev. D **39**, 3804 (1989).
[40] J. M. Lattimer, M. Prakash, C. J. Pethick, and P. Haensel, Phys. Rev. Lett. **66**, 2701 (1991).
[41] C. Cutler, L. Lindblom, and R. J. Splinter, Astrophys. J. **363**, 603 (1990).
[42] E. Flowers and N. Itoh, Astrophys. J. **206**, 218 (1976).
[43] P. S. Shternin and D. G. Yakovlev, Phys. Rev. D **78**, 063006 (2008).
[44] H. Heiselberg and C. J. Pethick, Phys. Rev. D **48**, 2916 (1993).
[45] J. L. Friedman and B. F. Schutz, Astrophys. J. **222**, 281 (1978).
[46] N. K. Glendenning, *Compact Stars: Nuclear Physics, Particle Physics, and General Relativity*, (Springer, Berlin, 2000).
[47] A. Reisenegger and A. A. Bonacic, Phys. Rev. Lett. **91**, 201103 (2003).
[48] E. F. Brown, L. Bildsten, and P. Chang, Astrophys. J. **574**, 920 (2002).
[49] R. N. Manchester, G. B. Hobbs, A. Teoh, and M. Hobbs, Astron. J. **129**, 1993 (2005).